NASA
Technical
Paper
2081

February 1983

A Method for Modifying Two-Dimensional Adaptive Wind-Tunnel Walls Including Analytical and Experimental Verification

Joel L. Everhart

NASA

NASA
Technical
Paper
2081

1983

A Method for Modifying Two-Dimensional Adaptive Wind-Tunnel Walls Including Analytical and Experimental Verification

Joel L. Everhart
Langley Research Center
Hampton, Virginia

NASA
National Aeronautics
and Space Administration
**Scientific and Technical
Information Branch**

SUMMARY

The theoretical development of a simple and consistent technique for removing the interference in adaptive-wall wind tunnels is reported. A Cauchy integral formulation of the velocities in an imaginary infinite extension of the real wind-tunnel flow is obtained and evaluated on a closed contour dividing the real and imaginary flow. The contour consists of the upper and lower effective wind-tunnel walls (wall plus boundary-layer displacement thickness) and upstream and downstream boundaries perpendicular to the axial tunnel flow. The resulting integral expressions for the streamwise and normal perturbation velocities on the contour are integrated by assuming a linear variation of the velocities between data-measurement stations along the contour. In an iterative process, the velocity components calculated on the upper and lower boundaries are then used to correct the shape of the wall to remove the interference. Convergence of the technique is shown numerically for the cases of a circular cylinder and a lifting and nonlifting NACA 0012 airfoil in incompressible flow. When starting from straight walls, convergence is achieved in three or four iterations if a relaxation factor of 0.25 is used when applying the predicted wall changes. Experimental convergence at a transonic Mach number is demonstrated by using an NACA 0012 airfoil at zero lift. Convergence of the experiment to within the wall-resolution capacity is achieved within three or four iterations.

INTRODUCTION

Because of the presence of the wind-tunnel walls, the flow about a model in a wind tunnel is constrained from that which would be experienced in the flow of free air about the same model. The experimental data acquired during a wind-tunnel test must then be adjusted (or corrected) in some manner to remove the effects of the wind-tunnel walls and, thus, give a valid representation of an unconstrained flow about the model. In the past, this has been attempted both empirically and theoretically. An example of an empirically derived correction in solid-wall wind tunnels would be to test two or more sizes of the same model in the wind tunnel to determine an appropriate ratio of model size to tunnel size for small wall effects. Likewise, in ventilated tunnels the wall-openness ratio for low interference may be determined by varying model size and tunnel-wall openness. The aforementioned empirical corrections are highly dependent on configuration and flow condition and, thus, are expensive in both time and money. Theoretical corrections have been developed and applied to help remove the empiricism. (See refs. 1 and 2.) When testing under modest wind-tunnel flow conditions, these classical corrections are uncertain; however, when testing under adverse conditions (i.e., high Mach number or low Mach number with high lift), they are unreliable.

To circumvent the required application of corrections to wind-tunnel data, the effective wind-tunnel wall, defined as the actual tunnel wall plus the boundary layer, may be contoured to the shape of the free-air streamlines about the model. Thus, a free-air test environment surrounds the model. The apparent fallacy of this approach is that it requires knowledge of the answer prior to the test.

In the early 1940's, Preston, et al., at the National Physical Laboratory, England, designed and tested a wind tunnel equipped with walls which could be adjusted to follow the streamlines about an airfoil model. (See refs. 3 and 4.)

These researchers defined an approximate method to adjust the walls which was based on singularities in the potential flow. Needless to say, their efforts, though notable, were not very successful because of the lack of theoretical development and numerical computational ability.

Kroeger and Martin (ref. 5) presented an approach for streamline modification to V/STOL wind tunnels in 1967. An analytical calculation was made and then a louvered wall was adjusted to provide aerodynamic relief to reduce the interference in the vicinity of the model. In 1972, Lo published a paper (ref. 6) which described a theoretical technique for reducing interference by applying an analytically obtained porosity distribution to the wind-tunnel walls prior to data acquisition. The porosity distribution calculated was a function of Mach number and, at least theoretically, allowed the streamwise gradient of lift interference to be removed and the blockage to be reduced.

In 1973, a method was proposed by which the streamline pattern around any object in a wind tunnel could be matched with that resulting from free air flow about the same object. This method, proposed by Ferri and Baronti (ref. 7) and also independently by Sears (ref. 8), is described as follows: an imaginary flow, satisfying the same free-stream reference as the real flow in the wind tunnel, is assumed to exist outside the physical boundaries of the wind tunnel. For unrestricted, interference-free flow to exist, the boundary conditions at the interface between the real and imaginary flows (the effective wind-tunnel wall) must be such that the boundary conditions governing the total flow (real plus imaginary) are those associated with free air, that is, the unperturbed conditions at infinity plus the conditions imposed on the test model. This is another way of stating that the imaginary flow is a continuous extension of the real flow to infinity. If two properties of the real flow are known at the wind-tunnel boundary, such as the pressure and streamline slope or the pressure and mass-flow rate, then one of the quantities may be used with the boundary condition at infinity to define the imaginary flow field. After this has been accomplished, the remaining quantity may be calculated analytically and compared with the experimentally determined value as a consistency check for the continuous extension of the real flow. If the two quantities match, the test model is in a free-air environment; if not, modifications to the real flow are made at the wind-tunnel boundary and the process is repeated until convergence to the free-air condition is achieved.

The aforementioned wall-interference reduction and/or elimination method presented has been implemented at several different research organizations around the world. Beginning in 1971, the Calspan Corporation started the development of an experimental wind tunnel to test the Ferri-Sears concept. Their tunnel was a two-dimensional-airfoil facility equipped with many plenum chambers along the upper and lower porous walls. The streamline contour was adjusted by varying the mass flow through the different plenum chambers. Results of their experiments presented in reference 9 showed convergence to near free air in about three successive iterations on the wall-control variables. Reference 9 also detailed some of their theoretical and numerical analyses along with their iterative method. Tunnel design and flow-field measurements were also discussed. Reference 10 discussed the extension of the Calspan work to high transonic Mach numbers and also the beginning of an investigation of a three-dimensional wind-tunnel design.

A test section with solid flexible walls was installed in the French ONERA S_4LCh wind tunnel (refs. 11 and 12) and was successfully used to remove wall-interference effects by controlling the streamline slope. The slope was integrated to give the streamline-shaped wall location. The French tests were conducted at transonic Mach

numbers under lifting and nonlifting conditions. Consideration was given to three-dimensional tunnels having solid flexible walls.

Another very extensive study, involving the University of Southampton, England, and the Langley Research Center, investigated the use of solid flexible walls for both low-speed and transonic wind tunnels. (See refs. 13 to 16.) The results of the low-speed studies (ref. 16) have been very encouraging with convergence in three or four iterations at any airfoil angle of attack when starting from straight (unstreamlined) walls and usually with convergence in one or two iterations when starting from a known solution at one angle of attack and moving to another angle of attack. (See ref. 15.) Theoretical studies of convergence, finite test-section effects, etc., were reported in reference 17. The use of the flexible-wall tunnel in other modes of operation is discussed in references 14 and 16. Among these are infinite flow field, cascade, ground effect, and steady pitching modes, thus indicating the utility and versatility of an adaptive-wall wind tunnel.

One of the main reasons for using the adaptive-wall principle, in addition to the reduction in interference that it offers, is the increase in test Reynolds number attainable because of the allowable increase in model size with respect to tunnel size and, correspondingly, the decrease in power requirements at a given Reynolds number. The Southampton tunnel, for instance, has a chord-height ratio of 0.90 and a tunnel height-width ratio of 0.50. The other tunnels cited have chord-height ratios of about 0.50 and height-width ratios of 1.20 or less. Typical two-dimensional-airfoil tunnels have chord-height ratios and height-width ratios of 0.33 or less and 3 or greater, respectively. Wolf and Goodyer (ref. 16) cited a possible problem area in adaptive-wall tunnel design by making the chord-height ratio too large. They attributed the disparity between their results and essentially interference-free results to a flexible-wall—boundary-layer interaction with the airfoil wake at large airfoil angles of attack.

In each of the aforementioned investigations of two-dimensional-airfoil tunnels with adaptive walls, the imaginary flow fields have been determined as two separate calculations on the upper and lower domains exterior to the upper and lower wind-tunnel walls. This manner of handling the iteration procedure decouples the calculations for opposing walls but does not decouple the effects of changes made to one wall on the opposing wall. Thus, excessive oscillation between walls can and does occur in the iteration procedure if the walls are not allowed to "communicate." In order to reduce the wall oscillation and, thus, the number of iterations, Wolf and Goodyer (ref. 15) introduced a correction method which summed a certain percentage of the movement of each of the opposing walls at each axial tunnel station. Likewise, to control the overshoot in the Calspan prediction, Sears (ref. 8) suggested applying only a percentage of the indicated wall change. Vidal, et al., (ref. 9) report that empirically determined relaxation factors of 0.25 were used.

As indicated previously, studies were made with independent calculations for the imaginary flow fields exterior to the upper and lower walls of the two-dimensional wind tunnel which decoupled the adjustment of the walls. Even though Chevallier (ref. 11) proposed that the imaginary flow should be calculated for a region exterior to a box containing the wind tunnel and that information obtained along the complete box contour be used for the calculation, he indicated in reference 12 that this procedure was not used and that separate upper and lower calculations were made. Each of these imaginary flows are determined on the half-plane, and they require information on boundaries extending to positive and negative infinity. Since the required information exists only along that portion of the boundary occupied by the wind tunnel, extrapolation of the known wall behavior must be made to satisfy the boundary

conditions. This procedure introduces an error of unknown magnitude into the iteration process. Analyses of the probable size of this error are given in references 12, 17, and 18.

The purpose of the present report is to present a coupled analytical and experimental method for eliminating the interference effects of the upper and lower wind-tunnel walls on an airfoil tested in a typical two-dimensional transonic wind tunnel with solid flexible floor and ceiling boundaries. An integral representation for the induced velocity along the wind-tunnel wall is developed and is evaluated by using data obtained on a closed contour composed of the upper and lower walls and upstream and downstream boundaries surrounding the model. An iterative technique is developed and experimental verification of the method is made for a nonlifting airfoil. A comparison is made with near-interference-free data and also with two different numerical simulations of the wind-tunnel geometry.

The theoretical and experimental investigation presented in this report was begun in early 1976 and was completed in 1977. The literature survey presented is indicative of the state of the art of adaptive-wall technology at the time of the investigation and does not include recent advances. When this work was completed, it was one of the first transonic adaptive-wall solutions and the only adaptive-wall theory applying Cauchy integral techniques. Between the time of completion of the test program and this publication, many advances have been made and similar theoretical approaches have been reported. The recent work of Kraft (ref. 19) is notable among the applications of the Cauchy integral techniques. Kraft applied the Cauchy integral to the interior of the wind tunnel to obtain expressions for the interference velocities, whereas the technique reported herein applies the Cauchy integral to the exterior of the wind tunnel to determine corrections to the wall boundary condition. A survey of past experience and recent technology applicable to adaptive walls was given at an AGARD symposium on "Wall Interference in Wind Tunnels" in May 1982.

SYMBOLS

A cross-sectional area of wind tunnel, in^2

A_i, A_D, A_P
B_i, B_D, B_P
C_i, C_D, C_P
D_j, E_j coefficients of discretized velocity integrals (where $i = 1,2,3$ and $j = 1,2$)

C_p pressure coefficient

c chord

c_l section lift coefficient

c_m section pitching-moment coefficient

c_1, c_2, c_3 different branches of contour of integration

F analytic function

I_1, I_2, I_3 definite integrals

i	imaginary number, $\sqrt{-1}$
ι_j	wall length between two data-measurement stations, in.
M	Mach number
n	number of measurement stations
P	running variable along wind-tunnel wall between measurement stations, in.
P_c	distance along singular strip to wall singularity, in.
P_j	location along wind-tunnel wall where a measurement station occurs, where $j = 1$ to n, in.
Φ	Cauchy principal value
q	quantity defined by equation (A27)
R	radial distance defined in figure 1, in.
R_{chord}	Reynolds number based on chord
R_x	Reynolds number based on x
R_{δ^*}	Reynolds number based on δ^*
r	distance from control point to running point of integration, in.
s,t	running coordinates
U	complex velocity, ft/sec
U_∞	free-stream velocity, ft/sec
U^+	complex velocity evaluated on c_1, ft/sec
u,v	x and y perturbation-velocity components, respectively, ft/sec
x,y	Cartesian coordinates in transformed plane
x_r,y_r	Cartesian coordinates in real plane
z	imaginary variable, $x + iy$
β	compressibility factor, $\sqrt{1 - M_\infty^2}$
γ	ratio of specific heats
$\Delta( )$	change in ( )
δ^*	boundary-layer displacement thickness, in.
ε	incremental limiting distance, in.

η, ξ coordinate difference defined by equations (16) and (15), respectively

Θ local wall slope, dy/dx, rad

ρ dummy variable of integration

τ angle defined in equation (10), rad

ϕ transformed perturbation-velocity potential

ϕ_r real perturbation-velocity potential

Subscripts:

c singular point

i,j indices of points, panels, etc.

o reference condition

r real flow

∞ free stream

Abbreviation:

rms root mean square

A prime indicates an arbitrary point on the contour.

PROBLEM FORMULATION

This report presents a method for reducing or removing the interference effects of the upper and lower walls of a two-dimensional wind tunnel. In this report, only the case of a steady, fully developed, two-dimensional fluid flow over an airfoil in a typical airfoil wind tunnel is considered. Although an airfoil is specified, the method is general enough that any two-dimensional object should not be excluded as long as restrictions (which are to be stated) are not violated.

The upper and lower wind-tunnel walls have a finite number of stations at which the vertical location of the wall can be controlled. The wall is assumed to be thin and flexible so that intermediate locations between the adjustment stations approximate a spline curve. If the wall approximates a streamline about the airfoil, the wall curvatures will not be excessive.

The effects of viscosity are considered to be confined to the region immediately adjacent to the four walls of the wind tunnel within the displacement thickness of the wall boundary layer. Viscous effects on the airfoil are unimportant to the analysis, except with regard to the relationship that they have with the development of the wake behind the airfoil. Since the thickness of the wake is generally small compared to the height of the tunnel, the viscous effects of the wake are not considered here.

The formation of shocks in the flow field within the wind tunnel is allowable; however, no provision is made for shock impingement on the upper and lower wind-tunnel walls. The method extends the real flow within the tunnel to infinity by introducing an imaginary flow exterior to the tunnel. The imaginary portion of the flow field is assumed to be isentropic even though shock waves may exist in the real flow. It is shown (ref. 20) that the terms affected by this assumption are of higher order than those to be considered in this analysis. Because of the isentropic assumption and the nature of the analysis, the equation governing the imaginary flow is taken as

$$(1 - M_\infty^2) \frac{\partial^2 \phi_r}{\partial x_r^2} + \frac{\partial^2 \phi_r}{\partial y_r^2} = 0 \tag{1}$$

where ϕ_r is the small perturbation-velocity potential and M_∞ is the free-stream Mach number. This is the linearized, two-dimensional, compressible-flow equation. The x_r coordinate is measured axially in the tunnel. The y_r coordinate is measured in the vertical direction. Boundary conditions for the real flow are the usual conditions of zero normal velocity at the airfoil surface and either the pressure or streamline slope at the effective walls of the wind tunnel. Boundary conditions for the imaginary flow exterior to the tunnel are the pressure distribution or streamline slope at the effective walls and vanishing perturbation velocities at infinity. In order to solve the coupled boundary-value problems consistently, however, both pressure and streamline slope should be specified.

METHOD OF ANALYSIS

The utilization of the Ferri-Sears concept requires the solution of equation (1) in the region exterior to the real flow in the wind tunnel. By using the following Goethert scaling rules:

$$\left.\begin{aligned} x &= x_r \\ y &= \beta y_r \\ u &= \beta^2 u_r \\ v &= \beta v_r \\ \phi &= \beta^2 \phi_r \end{aligned}\right\} \tag{2}$$

equation (1) becomes

$$\frac{\partial^2 \phi}{\partial x^2} + \frac{\partial^2 \phi}{\partial y^2} = 0 \tag{3}$$

Thus, the imaginary flow can be determined by using standard potential-flow techniques.

Development of Integral Representation of Velocity Field at Boundary

Since the shock waves do not extend to (or beyond) the walls of the wind tunnel, the function ϕ is assumed to be continuous. Because irrotational flow is assumed, the velocity components u and v are obtained from

$$u = \frac{\partial \phi}{\partial x} \tag{4}$$

and

$$v = \frac{\partial \phi}{\partial y} \tag{5}$$

As a result of the preceding argument, the functions u and v and their derivatives are assumed to be continuous. By appropriate differentiation of equations (4) and (5), u and v may be shown to satisfy the Cauchy-Riemann conditions and also the Laplace equation. Thus, they satisfy requirements for harmonic functions. (See ref. 21.) These functions may then be used to define a new function $U(z)$ which is analytic (ref. 21) in the domain exterior to the wind tunnel and which also satisfies the Laplace equation. The function $U(z)$ is given by the expression

$$U(z) = u(x,y) - i\, v(x,y) \tag{6}$$

In general, if any function $F(z)$ is analytic on and within a simple closed contour such as that represented in figure 1, the Cauchy integral formula (ref. 21) may be used to determine the value of $F(z)$ at any point $z = x + iy$ within the domain. The Cauchy integral formula is given by

$$F(z) = \frac{1}{2\pi i} \oint \frac{F(\rho)\, d\rho}{\rho - z} \tag{7}$$

where z is the location at which the value of F is desired and ρ is the dummy variable of integration. Examination of equation (7) reveals that the determination of $F(z)$ requires knowledge of the values of $F(z)$ occurring on the boundaries of the given analytic domain, that is, $F(\rho)$.

In order to replace $F(z)$ in equation (7) with $U(z)$ given in equation (6), the behavior of u and v on all boundaries must be known. If contour c_1 of figure 1 is taken as the control surface, then u and v are known measured quantities. For a flexible-wall tunnel, this surface is taken to be coincident with the upper and lower effective walls of the wind tunnel and is closed by two planes perpendicular to the undisturbed flow in the tunnel, one located ahead of the model and one behind the model. Boundary data along c_2 are not required because the influ-

ence of these data is cancelled. If contour c_3 is taken as the limit of R going to infinity, then u and v on c_3 will vanish since the perturbations vanish at infinity. Equation (7) is then rewritten as:

$$U(z) = \frac{1}{2\pi i}\left(\oint_{c_1} + \int_{c_2} + \oint_{c_3} - \int_{c_2}\right)\left[\frac{U(\rho)\, d\rho}{\rho - z}\right] = \frac{1}{2\pi i}\oint_{c_1}\frac{U(\rho)\, d\rho}{\rho - z} \tag{8}$$

It is important to note that the region labeled "Singular region" in figure 1 comprises the area contained within the effective walls of the wind tunnel and outside the contour c_1. The airfoil and tunnel conditions impose a pressure distribution along the walls of the contour, which gives rise to a perturbation-velocity field. The exact nature of the flow is unknown. Information is not known or needed on shock-wave formation, the model test configuration, and conditions of this type.

As stated earlier, equation (8) will give values of the velocity function U(z) within the analytic domain. In order to obtain values $U^+(z)$ on the contour, a limiting process must be applied to equation (8). Figure 2 shows the contour over which the limiting process occurs as z approaches c_1 from the interior and defines the symbols used in the formulation. Equation (8), when written over the contour in figure 2, is

$$U^+(z) = \lim_{\varepsilon \to 0}\left[\frac{1}{2\pi i}\oint_{c_1 - \varepsilon}\frac{U(\rho)\, d\rho}{\rho - z} + \frac{1}{2\pi i}\int_{\varepsilon}\frac{U(\rho)\, d\rho}{\rho - z}\right] \tag{9}$$

Using the definition

$$\rho - z = \varepsilon e^{i\tau} \qquad (0 \leq \tau \leq \pi) \tag{10}$$

allows the last integral in equation (9) to be expressed as

$$\lim_{\varepsilon \to 0}\frac{1}{2\pi i}\int_{\varepsilon}\frac{U(\rho)\, d\rho}{\rho - z} = \lim_{\varepsilon \to 0}\frac{1}{2\pi}\int_0^{\pi} U(z + \varepsilon e^{i\tau})\, d\tau = \frac{U^+(z)}{2} \tag{11}$$

Then, substituting equation (11) into (9) gives

$$U^+(z) = \frac{1}{\pi i}\Phi\oint_{c_1}\frac{U(\rho)\, d\rho}{\rho - z} \tag{12}$$

for values of $U(z)$ when z is on the contour c_1 (the wind-tunnel-wall contour), that is, $U^+(z)$. The real and imaginary portions of $U^+(z)$ are obtained by making the following substitutions into equation (12):

$$z = x + iy \tag{13}$$

$$\rho = s + it \tag{14}$$

$$\xi = s - x \tag{15}$$

$$\eta = t - y \tag{16}$$

$$r^2 = \xi^2 + \eta^2 \tag{17}$$

and equation (6). After manipulation, the u and v components of the perturbation velocity evaluated on the contour c_1 become, respectively,

$$u(x,y) = -\frac{1}{\pi} \Phi \oint_{c_1} \frac{(u\eta + v\xi)ds - (u\xi - v\eta)dt}{r^2} \tag{18}$$

and

$$v(x,y) = \frac{1}{\pi} \Phi \oint_{c_1} \frac{(u\xi - v\eta)ds + (u\eta + v\xi)dt}{r^2} \tag{19}$$

Note that the superscript + (denoting limiting value on the contour) has been deleted from u and v for convenience. The results of equations (18) and (19) can be transformed back to the compressible plane by using equations (2).

Treatment of Boundary Data

The information collected at the control surface c_1 is usually in the form of pressure and flow angle. These quantities are converted to the velocities u_r and v_r by using

$$C_{p,r} = \frac{2}{\gamma M_\infty^2}\left\{\left[1 - \left(\frac{\gamma - 1}{2}\right)M_\infty^2\left(\frac{U_r^2}{U_\infty^2} - 1\right)\right]^{\frac{\gamma}{\gamma-1}} - 1\right\} \tag{20}$$

and

$$\Theta_r = \frac{v_r}{U_\infty + u_r} = \left.\frac{dy_r}{dx_r}\right|_{c_1} \tag{21}$$

where $C_{p,r}$ is the pressure coefficient and $\left.\frac{dy_r}{dx_r}\right|_{c_1}$ is the (assumed small) flow angle with respect to the free stream at the control surface; that is, $\Theta_r \approx \tan \Theta_r$.

Contour Adjustment to Reduce Wall Interference

The Ferri-Sears iteration requires measurement of two flow quantities. One of these is used to calculate an imaginary extension of the real flow to infinity; the other is used as a consistency check with its imaginary counterpart. In the present method, the u and v components of the velocity at the control surface are obtained from equations (20) and (21) and then are used to evaluate equations (18) and (19) in order to calculate the streamline slope in the exterior flow. This slope is integrated to obtain a new wall position, and the calculated value is then compared with the corresponding measured value to determine if continuity exists between the real and imaginary flows. If a discrepancy exists between the measured and calculated contours, the contour is moved and the process is then repeated. If the error is reduced to an acceptable level, convergence is declared and the measured wind-tunnel data should be correct to within definable limits of accuracy.

It is important to note that if changes are made at one location on the wall, the effects of this change are felt globally in the tunnel unless the change is very small. Thus, the walls should not be decoupled during exterior-flow calculations. The present method allows communication between the walls and should tend to reduce the oscillation present in other methods, although a relaxation of the calculated correction will most likely have to be applied.

COMPUTER PROGRAM FOR WIND-TUNNEL-WALL ANALYSIS

To apply the analysis of the preceding sections, equations (18) and (19) must be reduced to a form suitable for numerical solution. Since speed and low cost are essential during any computer operation occurring while running a wind tunnel, simple methods must be used. It is assumed that the pressure data obtained on the wall are dense enough that a linear variation of the velocity components between measurement stations will reflect their true variation. It is also assumed that the shape of the wall between the adjustment stations will approximate a spline curve so that any intermediate wall location and slope may be determined from the spline fit of the wall ordinates. With these two approximations in the integrands of equations (18) and (19), the velocity integrals may be simplified and evaluated along strips between pressure-measurement stations. The effects of each of these strips are then summed over the entire contour, which results in a value of the induced velocity at each of the adjustment stations along the effective wind-tunnel-wall contour c_1. The discretization of the equations is shown in detail in the appendix, and a computer program called "FLEXWAL" has been written to implement the method.

RESULTS

The general application of the method was described in the preceding sections. The specific details of its use will be described in the following sections along with numerical and experimental verification. The experimental results will be compared with experimental data and also with a wall shape obtained by a different method.

Numerical Demonstration of Convergence

The convergence properties of the concept were studied numerically for three incompressible test cases: a circular cylinder, a nonlifting NACA 0012 airfoil, and an NACA 0012 airfoil at an angle of attack of 3°. The pressure distribution imposed along the wind-tunnel walls during the numerical studies was obtained by using the MAAD computer program described in reference 22. This program solves the inviscid, incompressible flow field about multielement airfoils using panel methods. To simulate walls, one element, which would normally be used for the airfoil, may be wrapped around the airfoil configuration to be analyzed. Various types of boundary conditions may be prescribed along the different surfaces, and either analysis or design cases may be computed. The MAAD program produces results in the form of pressure distributions along the walls and airfoil surface. The force coefficients are derived from the integration of the pressures.

In each of the test cases the chord-height ratio was chosen as 0.5 to provide a severe test of the method, and all iterations were started from straight undiverged walls. Boundary conditions of vanishing normal velocity were prescribed along the upper and lower tunnel walls and along the airfoil surface. The tunnel walls were extended far enough upstream and downstream of the model to allow the vertical-velocity components to be neglected and, thus, a free-stream velocity of unity was prescribed. Wall pressures generated by the MAAD program and the existing wall shape were then used as input to the FLEXWAL program. Results from the FLEXWAL program were in the form of Δy corrections at the wall-adjustment locations. These new wall locations were then used as input to the MAAD program, and the process was repeated.

The convergence properties of the method for a circular cylinder are presented in figure 3. Here, the root mean square (rms) of the predicted wall correction normalized by the rms value of the first prediction is plotted against the iteration number for various values of wall relaxation. If the full predicted correction is used, then an unstable situation exists and the method diverges rapidly. However, if only 25 percent of the correction is applied, the maximum convergence rate is achieved. This is consistent with the results of reference 9. Figure 4 presents the wall shapes obtained by using an under relaxation factor of 0.25 of the predicted Δy correction. Very little change occurs after the third iteration, and essentially no change occurs after the fourth iteration.

The convergence characteristics were then studied for both a nonlifting and lifting NACA 0012 airfoil, and the wall results are presented in figure 5. Two interesting points are noticeable here. First, the convergence of both of these cases is slower than that of the circular cylinder in figure 3. This is due to the lack of streamwise symmetry in the pressure distribution as compared with that of the circular cylinder. Second, the upper and lower walls of the lifting configuration converge at the same rate. Further studies with the method should be conducted before making any profound statements about the generality of this.

Convergence of the force coefficients for the lifting airfoil is presented in figure 6, which shows a comparison with a reference free-air calculation obtained by removing the walls in the MAAD computer program. It is observed that although the walls are converged after three or four iterations, the error in force coefficients is reduced to less than 3 percent by the second iteration.

At this point, it should be noted that the convergence could have been enhanced if a less severe test case had been chosen. If the chord-height ratio of the tunnel was more in line with those of typical airfoil tunnels, the velocities induced on the walls by the airfoil would have been smaller and, thus, the wall corrections would have been correspondingly less. Also, since all iterations were started from undiverged walls, the iterations required for convergence would be less if they were started from, say, a converged 2° angle-of-attack case and were iterated to a converged 3° angle-of-attack case.

Experimental Verification of Convergence

An experimental study of the flexible-wall iteration procedure was conducted in the Langley 6- by 19-Inch Transonic Tunnel. (See ref. 23.) The wind tunnel is an atmospheric blowdown facility with 0.0125-open slotted upper and lower walls. It has a Mach number range from about 0.2 to 1.2 and a Reynolds number capability of about 3.0×10^6, based on an airfoil chord of 6 in. The airfoil model spans the tunnel and is mounted rigidly on turntables which are manually rotated to change angle of attack. A typical test run would consist of a Mach number sweep at a fixed airfoil angle of attack.

For the present study, the slotted upper and lower walls were removed and replaced with solid flexible walls extending from 29 in. ahead of to 20 in. behind the airfoil model. Each wall had 11 manually operated jacking stations equally spaced at 4-in. intervals, where the wall location could be adjusted to within about ±0.0015 in. of the desired setting. There were 20 center-line pressure orifices along each upper and lower wall. Tunnel center-line pressure orifices were installed along the sidewall both upstream and downstream of the model. A vertical row of 5 orifices located 30 in. upstream of the airfoil midchord was used as a reference for the wind-tunnel Mach number.

The model selected for the study was an NACA 0012 airfoil having a 6-in. chord. The model has 45 pressure orifices distributed equally on the upper and lower surfaces with 1 located in the leading edge. The model is mounted between tunnel stations -3 in. and 3 in. All measurements were obtained at zero angle of attack. No drag data were obtained during any of the test runs. A schematic drawing of the facility and the flexible wall is shown in figure 7.

Corrections to the flexible walls to remove interference were made in three phases. Phase I was a tunnel-empty boundary-layer correction. In this phase, the walls were diverged to obtain a level pressure distribution along the tunnel axis. This was accomplished by using the area-ratio expression

$$\frac{A}{A_o} = \frac{M_o}{M}\left(\frac{1 + \frac{\gamma - 1}{2} M^2}{1 + \frac{\gamma - 1}{2} M_o^2}\right)^{\frac{\gamma+1}{2(\gamma-1)}}$$

obtained from one-dimensional gas dynamics. Here, A and M are the local area and Mach number, respectively, and A_o and M_o are the upstream reference conditions of the same quantities, respectively. After the local area change was determined, an approximate value of the local change in the displacement thickness $\Delta\delta^*$ was calculated from

$$\Delta\delta^* \approx \frac{6 \times 19}{2(6 + 19)} \left(1 - \frac{A}{A_o}\right)$$

Since the sidewalls of the tunnel are rigid, all corrections were applied equally to the top and bottom flexible walls. The Δy correction was determined by using

$$\Delta y = \frac{6 + 19}{6} \Delta\delta^*$$

The results of this procedure for a Mach number of about 0.71 are presented in figure 8, in which pressure data obtained along both flexible walls and the tunnel center line are plotted for the undiverged and diverged tunnel-wall configurations. It is noted that the walls were diverged for a Mach number of 0.90, but this setting was equally valid across the Mach number range as shown in figure 9. The tunnel-empty boundary-layer growth was assumed to vary as

$$\frac{\delta^*}{x} = \frac{a}{R_x^b}$$

along each wall. The coefficients a and b were determined to have the values of 0.0643 and 1/5, respectively, by empirically matching the measured wall deflections required to achieve a constant Mach number distribution in the test section. The corrections are shown in figure 10.

The Phase II wall corrections were modifications to account for model-imposed pressure-gradient variations of the wall boundary layer. Differentiating the previously noted expression for δ^* will yield

$$\frac{d\delta^*}{dx} = \frac{0.259}{R_{\delta^*}^{1/4}}$$

If the pressure-gradient term from the momentum integral equation is added and if the shape factor is assumed to have the value of 1.4, that is, the value typically assumed for a flat plate, then a generalized expression of the boundary-layer variation is given by

$$\frac{d\delta^*}{dx} + (3.4 - M^2) \frac{\delta^*}{u} \frac{du}{dx} = \frac{0.259}{R_{\delta^*}^{1/4}}$$

The previous equation was then incorporated into a computer program which solves the transonic small-disturbance flow about an airfoil. Integration of this equation was then made along two-dimensional strips on all four of the tunnel walls to obtain the model-imposed pressure-gradient effects on the displacement thickness. The theoretical viscous modifications of Phase II are also shown in figure 10. The corrections to the flat-plate growth thus obtained were then added to those of Phase I to yield the effective straight-wall settings, that is, the actual wall location plus the δ^* variation due to the model pressure field. Figure 11 presents the results of the aforementioned wall modification by comparing the airfoil pressure distribution obtained with the tunnel-empty wall settings with the airfoil pressure distribution obtained with the effective straight-wall settings at a free-stream Mach number of 0.77. It can be seen that the straight walls force an aftward movement of the shock, which is indicative of the effects of a closed tunnel.

The final phase (Phase III) consisted of potential-flow corrections in the manner described in the analysis section. The iterations were started from the effective straight-wall settings, and a Mach number of 0.767, as measured from the upstream reference, was taken as the free-stream test condition. At this Mach number, a Reynolds number of about 3.0×10^6 could be obtained in the test facility. Because a symmetrical nonlifting model was used, the pressures on the upper and lower walls at each given tunnel station were averaged to reduce experimental scatter in the data. This gave symmetrical upper and lower wall corrections which are presented in figure 12. The results identified as 2A represent 12.5 percent of the full correction predicted from iteration 1. Analysis of the pressure data from 2A with the FLEXWAL program indicated that ahead of and over the model, an inward movement of the wall would be required for the next iteration. The results identified as 2B represent 25 percent of the full correction predicted from iteration 1.

Analysis of the pressure data from 2B with the FLEXWAL program indicated that an outward movement of the wall over the same region would be required for the next iteration. Thus, the converged location for most of the wall should lie between that of iterations 2A and 2B. Based on this, it was decided to interpolate between iterations 2A and 2B by using the actual wall location and the predicted wall changes from both runs 2A and 2B. The results of this are indicated as iteration 3. It is seen from figure 12 that there is very little difference in the wall positions between iterations 2B and 3. The major differences appear to start about 1-chord length downstream of the model trailing edge and extend to the end of the flexible-wall test section. It is thought that these discrepancies are the result of the inefficient dumping of air leaving the test section and flowing into the diffuser and possibly the result of insufficient control of the walls in this region. A post-test evaluation of the flexible-wall error analysis is given in the following table:

Iteration	Relaxation factor	rms	$\frac{\text{rms}}{(\text{rms})_o}$
0		0.08907	1
1	0.250	.03295	.36997
2A	.125	.02316	.26000
2B	.250	.02201	.24716
3	Interpolated	.01251	.14043

The walls are converging as found in the numerical example, although not at the optimum rate. (See fig. 3.)

The convergence of the airfoil pressure data is presented in figure 13. It can be seen that very little difference exists in data obtained from iterations 2A, 2B, and 3. The differences that are present, essentially a very small shift in the shock location, are within the Mach number and data scatter. Thus, for all practical purposes, convergence is achieved for this test configuration.

COMPARISON OF FINAL RESULTS WITH OTHER DATA

In this section, the final results presented in figures 12 and 13 are compared with other data and procedures. Figure 14 shows the agreement between the wall shape obtained by the present method and that obtained by the analytical method of Newman and Anderson. (See refs. 24 and 25.) Their technique solves the direct, inviscid boundary-value problem for the free air flow about the shape given by an NACA 0012 airfoil plus its boundary-layer displacement thickness. The tunnel-wall boundary-layer correction is then computed in a two-dimensional stripwise sense along all bounding streamlines and is added to the inviscid streamline displacement to give the solid contoured tunnel-wall shape. For comparison purposes, all tunnel-wall boundary-layer displacement effects were added symmetrically to the top and bottom inviscid wall deflections. It can be seen that there is a substantial difference between the viscous and inviscid predictions. A splined curve through the actual tunnel-wall location (viscous flow plus potential-flow corrections) from the present study is in good agreement with the theoretical viscous prediction over most of the wall. If the fine detail of the theoretical viscous prediction is valid, then it is obvious that the wall jacks are too sparse to approximate the required shape. However, it is very encouraging to see how well the required wall shape is approximated experimentally. The downstream discrepancy (as stated earlier) occurs because of the inefficient dumping of the tunnel air into the diffuser and possibly because of insufficient wall control.

Figure 15 compares the converged airfoil pressure distribution with unpublished experimental data obtained by J. Osborne of the Royal Aircraft Establishment, England. Osborne determined the blockage interference on an NACA 0012 airfoil at zero lift in the 36- by 14-inch two-dimensional transonic wind tunnel at the National Physical Laboratory. During the Osborne test, the wall openness was systematically varied to determine the correct value in such a way that identical pressures could be obtained over the 15- to 55-percent chord region of both a 5-in. and a 10-in. model at identical free-stream Mach numbers. It is seen that the data match reasonably well over most of the airfoil with the largest difference being at the shock. If the Osborne data are considered to be correct, then the results of the present study appear to have been obtained in a wind tunnel which is too open. This is consistent with the findings presented in figure 14; that is, the location (or slope) of the wall is not adequately controlled in the immediate vicinity of the shock above the airfoil because the wall is too open there.

CONCLUDING REMARKS

When the wall-iteration—convergence concepts used in this report were originally conceived, the computational procedures for modeling the wind-tunnel flow were not generally available and, thus, verification of the theoretical ideas and wall-construction geometry was difficult. With the advent of the MAAD computer code, an

incompressible tool for analysis of the method became available and the convergence characteristics of the method could be easily studied. It has been shown analytically and computationally that convergence for the severe case of the ratio of model chord to tunnel height of 0.5 could be achieved in three or four iterations for incompressible lifting and nonlifting models when starting from straight undiverged walls. The number of iterations should be reduced substantially if wall modifications begin at a previously adapted wall shape and/or if the model-tunnel geometry is less demanding. The method also demonstrated a proper coupling of the upper and lower tunnel walls contrary to other methods; however, under relaxation of the predicted wall change is required, and a relaxation factor of 0.25 gave the maximum convergence rate in the numerical examples.

Experimental verification has been demonstrated at a low transonic Mach number for symmetric flow to within the wall-resolution capabilities in two or three iterations. It is important to note that although the jack spacing on the test wall was adequate for the inviscid streamline modification, the spacing was unacceptable for capturing the required fine details because of the boundary-layer variation on the sidewalls. For the particular test case studied, this lack of boundary-layer definition appears to have manifested itself in the improper location and strength of the airfoil shock wave.

Langley Research Center
National Aeronautics and Space Administration
Hampton, VA 23665
December 22, 1982

APPENDIX

DISCRETIZATION OF PERTURBATION-VELOCITY INTEGRALS

For reference, the perturbation-velocity integral and related expressions are

$$u(x,y) = -\frac{1}{\pi} \Phi \oint_{C_1} \frac{(u\eta + v\xi)ds - (u\xi - v\eta)dt}{r^2} \tag{A1}$$

and

$$v(x,y) = \frac{1}{\pi} \Phi \oint_{C_1} \frac{(u\xi - v\eta)ds + (u\eta + v\xi)dt}{r^2} \tag{A2}$$

where

$$\left.\begin{aligned} \xi &= s - x \\ \eta &= t - y \\ r^2 &= \xi^2 + \eta^2 \end{aligned}\right\} \tag{A3}$$

The closed path over which the integration occurs is shown in figure 16(a). The contour is composed of a finite number of discrete points at which information is known. These data points are denoted by the symbol P_j, where the subscript j is an index denoting the point being considered. The wall is assumed to be composed of straight-line segments between successive data points as shown in figure 16(b). The point labeled with the subscript i is the location at which the integrals are evaluated. The length of each segment is

$$l_j = [(s_{j+1} - s_j)^2 + (t_{j+1} - t_j)^2]^{1/2} \tag{A4}$$

By using equation (A4), running coordinates may be established along each segment. Thus,

$$s(P') = s_j + (s_{j+1} - s_j)\frac{P' - P_j}{l_j}$$

and

$$t(P') = t_j + (t_j - t_j)\frac{P' - P_j}{\ell_j}$$

However, if

$$P = P' - P_j$$

then

$$s(P) = s_j + (s_{j+1} - s_j)\frac{P}{\ell_j} \tag{A5}$$

and

$$t(P) = t_j + (t_{j+1} - t_j)\frac{P}{\ell_j} \tag{A6}$$

where P varies from 0 for $P' = P_j$ to ℓ_j for $P' = P_{j+1}$. Likewise, by assuming a linear variation in u and v along each strip, the velocities are written as

$$u(P) = u_j + (u_{j+1} - u_j)\frac{P}{\ell_j} \tag{A7}$$

and

$$v(P) = v_j + (v_{j+1} - v_j)\frac{P}{\ell_j} \tag{A8}$$

By differentiation of equations (A5) and (A6),

$$ds = \frac{s_{j+1} - s_j}{\ell_j}\, dP \tag{A9}$$

and

$$dt = \frac{t_{j+1} - t_j}{\ell_j}\, dP \tag{A10}$$

APPENDIX

The expression for $r^2(P)$ is developed by using

$$s - x_i = -(x_i - s_j) + (s_{j+1} - s_j)\frac{P}{\ell_j} \tag{A11}$$

and

$$t - y_i = -(y_i - t_j) + (t_{j+1} - t_j)\frac{P}{\ell_j} \tag{A12}$$

Thus,

$$r^2(P) = [(x_i - s_j)^2 + (y_i - t_j)^2] - 2[(x_i - s_j)(s_{j+1} - s_j) + (y_i - t_j)(t_{j+1} - t_j)]\frac{P}{\ell_j} + P^2 \tag{A13}$$

By using equations (A7), (A8), (A11), and (A12), the following relations are obtained:

$$(s - x_i)u = -u_j(x_i - s_j) + [(s_{j+1} - s_j)u_j - (x_i - s_j)(u_{j+1} - u_j)]\frac{P}{\ell_j} + (s_{j+1} - s_j)(u_{j+1} - u_j)\left(\frac{P}{\ell_j}\right)^2 \tag{A14}$$

$$(t - y_i)u = -u_j(y_i - t_j) + [(t_{j+1} - t_j)u_j - (y_i - t_j)(u_{j+1} - u_j)]\frac{P}{\ell_j} + (t_{j+1} - t_j)(u_{j+1} - u_j)\left(\frac{P}{\ell_j}\right)^2 \tag{A15}$$

$$(s - x_i)v = -v_j(x_i - s_j) + [(s_{j+1} - s_j)v_j - (x_i - s_j)(v_{j+1} - v_j)]\frac{P}{\ell_j} + (s_{j+1} - s_j)(v_{j+1} - v_j)\left(\frac{P}{\ell_j}\right)^2 \tag{A16}$$

$$(t - y_i)v = -v_j(y_i - t_j) + [(t_{j+1} - t_j)v_j - (y_i - t_j)(v_{j+1} - v_j)]\frac{P}{\ell_j} + (t_{j+1} - t_j)(v_{j+1} - v_j)\left(\frac{P}{\ell_j}\right)^2 \tag{A17}$$

APPENDIX

By defining

$$A_1 = -u_j(x_i - s_j) \tag{A18a}$$

$$A_2 = -v_j(x_i - s_j) \tag{A18b}$$

$$A_3 = -u_j(y_i - t_j) \tag{A18c}$$

$$A_4 = -v_j(y_i - t_j) \tag{A18d}$$

$$B_1 = \frac{(s_{j+1} - s_j)u_j - (x_i - s_j)(u_{j+1} - u_j)}{l_j} \tag{A18e}$$

$$B_2 = \frac{(s_{j+1} - s_j)v_j - (x_i - s_j)(v_{j+1} - v_j)}{l_j} \tag{A18f}$$

$$B_3 = \frac{(t_{j+1} - t_j)u_j - (y_i - t_j)(u_{j+1} - u_j)}{l_j} \tag{A18g}$$

$$B_4 = \frac{(t_{j+1} - t_j)v_j - (y_i - t_j)(v_{j+1} - v_j)}{l_j} \tag{A18h}$$

$$C_1 = \frac{(s_{j+1} - s_j)(u_{j+1} - u_j)}{l_j^2} \tag{A18i}$$

$$C_2 = \frac{(s_{j+1} - s_j)(v_{j+1} - v_j)}{l_j^2} \tag{A18j}$$

$$C_3 = \frac{(t_{j+1} - t_j)(u_{j+1} - u_j)}{l_j^2} \tag{A18k}$$

$$C_4 = \frac{(t_{j+1} - t_j)(v_{j+1} - v_j)}{l_j^2} \tag{A18l}$$

$$D_1 = (x_i - s_j)^2 + (y_i - t_j)^2 \tag{A18m}$$

$$D_2 = -\frac{2}{l_j}[(s_{j+1} - s_j)(x_i - s_j) + (t_{j+1} - t_j)(y_i - t_j)] \tag{A18n}$$

$$E_1 = \frac{s_{j+1} - s_j}{l_j} \tag{A18o}$$

$$E_2 = \frac{t_{j+1} - t_j}{l_j} \tag{A18p}$$

$$A_P = A_2 + A_3 \tag{A18q}$$

$$B_P = B_2 + B_3 \tag{A18r}$$

$$C_P = C_2 + C_3 \tag{A18s}$$

$$A_D = A_1 - A_4 \tag{A18t}$$

$$B_D = B_1 - B_4 \tag{A18u}$$

$$C_D = C_1 - C_4 \tag{A18v}$$

the integrals in equations (A1) and (A2) are rewritten as

$$u(x_i, y_i) = -\frac{1}{\pi}\sum_{j=1}^{n}\left(E_1\Phi\int_0^{l_j}\frac{A_P + B_P P + C_P P^2}{D_1 + D_2 P + P^2}\,dP - E_2\Phi\int_0^{l_j}\frac{A_D + B_D P + C_D P^2}{D_1 + D_2 P + P^2}\,dP\right) \tag{A19}$$

and

$$v(x_i, y_i) = \frac{1}{\pi}\sum_{j=1}^{n}\left(E_1\Phi\int_0^{l_j}\frac{A_D + B_D P + C_D P^2}{D_1 + D_2 P + P^2}\,dP + E_2\Phi\int_0^{l_j}\frac{A_P + B_P P + C_P P^2}{D_1 + D_2 P + P^2}\,dP\right) \tag{A20}$$

APPENDIX

The integrals in equations (A19) and (A20) are of the form

$$\int_0^{l_j} \frac{A + BP + CP^2}{D_1 + D_2P + P^2}\, dP = AI_1 + BI_2 + CI_3 \tag{A21}$$

where

$$I_1 = \int_0^{l_j} \frac{dP}{D_1 + D_2P + P^2} \tag{A22}$$

$$I_2 = \int_0^{l_j} \frac{P\, dP}{D_1 + D_2P + P^2} \tag{A23}$$

$$I_3 = \int_0^{l_j} \frac{P^2\, dP}{D_1 + D_2P + P^2} \tag{A24}$$

Thus,

$$u(x_i,y_i) = -\frac{1}{\pi} \sum_{j=1}^{n} [E_1(A_PI_1 + B_PI_2 + C_PI_3) - E_2(A_DI_1 + B_DI_2 + C_DI_3)] \tag{A25}$$

and

$$v(x_i,y_i) = \frac{1}{\pi} \sum_{j=1}^{n} [E_1(A_DI_1 + B_DI_2 + C_DI_3) + E_2(A_PI_1 + B_PI_2 + C_PI_3)] \tag{A26}$$

When using the integral tables for evaluating the integrals in equations (A22), (A23), and (A24), care must be taken to choose the appropriate integration formula. This requires examination of the sign and value of the quantity q, which is defined as

$$q = 4D_1 - D_2^2$$

$$= \frac{4}{l_j^2}[(x_i - s_j)(t_{j+1} - t_j) - (y_i - t_j)(s_{j+1} - s_j)]^2 \tag{A27}$$

Therefore,

$$q > 0 \tag{A28}$$

APPENDIX

By using the integral tables of reference 26, the following equations can be written: For $q > 0$,

$$I_1 = \frac{2}{\sqrt{q}} \tan^{-1}\left(\frac{\iota_j\sqrt{q}}{2D_1 + \iota_j D_2}\right) \tag{A29}$$

$$I_2 = \frac{1}{2} \ln\left(\frac{D_1 + D_2\iota_j + \iota_j^2}{D_1}\right) - \frac{D_2}{2} I_1 \tag{A30}$$

$$I_3 = \iota_j - D_2 I_2 - D_1 I_1 \tag{A31}$$

If

$$q = 4D_1 - D_2^2 = 0$$

then

$$D_1 = \left(\frac{D_2}{2}\right)^2$$

which gives

$$I_1 = \frac{\iota_j}{\frac{D_2}{2}\left(\frac{D_2}{2} + \iota_j\right)} \tag{A32}$$

$$I_2 = \ln\left(\frac{\frac{D_2}{2} + \iota_j}{\frac{D_2}{2}}\right) - \frac{D_2}{2} I_1 \tag{A33}$$

$$I_3 = \iota_j - D_2 I_2 - \left(\frac{D_2}{2}\right)^2 I_1 \tag{A34}$$

Examination of the integral expressions given in equations (A1) and (A2) or (A19) and (A20) shows that a singularity exists along the strip containing the point

$r^2 = 0$. Along this portion of the contour, then, the Cauchy principal part of the integral must be used. By considering the geometry as shown in figure 16(b), it can be seen that

$$\frac{\xi}{r} = \frac{s_{j+1} - s_j}{\ell_j} = E_1 \tag{A35}$$

$$\frac{\eta}{r} = \frac{t_{j+1} - t_j}{\ell_j} = E_2 \tag{A36}$$

The integrals along the strip containing the singularity are then rewritten as

$$u = -\frac{1}{\pi} \Phi \int_{s_j}^{s_{j+1}} \frac{uE_2 + vE_1}{r} ds + \frac{1}{\pi} \Phi \int_{t_j}^{t_{j+1}} \frac{uE_1 - vE_2}{r} dt \tag{A37}$$

and

$$v = \frac{1}{\pi} \Phi \int_{s_j}^{s_{j+1}} \frac{uE_1 - vE_2}{r} ds + \frac{1}{\pi} \Phi \int_{t_j}^{t_{j+1}} \frac{uE_2 + vE_1}{r} dt \tag{A38}$$

by using the notation shown in figure 16(c), which has P_j and P_{j+1} at the ends of the strip, P' as the running point along the strip, and P'_c as the location of the singularity. Then,

$$\begin{aligned} r &= P' - P'_c \\ &= P' - P_j - P'_c + P_j \\ &= (P' - P_j) - (P'_c - P_j) \end{aligned}$$

or, according to previous usage,

$$r = P - P_c \tag{A39}$$

The singular-strip integrals in equations (A37) and (A38) are then rewritten with the aid of equations (A7) to (A10) and (A39) as

$$u_c = -\frac{1}{\pi} \Phi \int_0^{l_j} \frac{v_j + (v_{j+1} - v_j)\frac{P}{l_j}}{P - P_c} \, dP \tag{A40}$$

and

$$v_c = \frac{1}{\pi} \Phi \int_0^{l_j} \frac{u_j + (u_{j+1} - u_j)\frac{P}{l_j}}{P - P_c} \, dP \tag{A41}$$

The integrands of equations (A40) and (A41) are rewritten, respectively, as

$$\left(v_j + P_c \frac{v_{j+1} - v_j}{l_j}\right)\frac{1}{P - P_c} + \frac{v_{j+1} - v_j}{l_j} \tag{A42}$$

and

$$\left(u_j + P_c \frac{u_{j+1} - u_j}{l_j}\right)\frac{1}{P - P_c} + \frac{u_{j+1} - u_j}{l_j} \tag{A43}$$

Then, by substituting equations (A42) and (A43) into (A40) and (A41), the integrals become

$$u_c = -\frac{1}{\pi}\left[\left(v_j + P_c \frac{v_{j+1} - v_j}{l_j}\right)\Phi \int_0^{l_j} \frac{dP}{P - P_c} + \frac{v_{j+1} - v_j}{l_j}\int_0^{l_j} dP\right] \tag{A44}$$

and

$$v_c = \frac{1}{\pi}\left[\left(u_j + P_c \frac{u_{j+1} - u_j}{l_j}\right)\Phi \int_0^{l_j} \frac{dP}{P - P_c} + \frac{u_{j+1} - u_j}{l_j}\int_0^{l_j} dP\right] \tag{A45}$$

The singularity now occurs in the first integral of each of equations (A44) and (A45). These are evaluated by taking the limits around P_c of

$$\lim_{\varepsilon \to 0} \left(\int_0^{P_c - \varepsilon} + \int_{P_c + \varepsilon}^{l_j} \frac{dP}{P - P_c} \right) = \ln \left(\frac{l_j - P_c}{P_c} \right) \tag{A46}$$

Substituting equation (A46) into (A44) and (A45) gives, respectively,

$$u_c = - \frac{1}{\pi} \left[\left(v_j + P_c \frac{v_{j+1} - v_j}{l_j} \right) \ln \left(\frac{l_j - P_c}{P_c} \right) + (v_{j+1} - v_j) \right] \tag{A47}$$

and

$$v_c = \frac{1}{\pi} \left[\left(u_j + P_c \frac{u_{j+1} - u_j}{l_j} \right) \ln \left(\frac{l_j - P_c}{P_c} \right) + (u_{j+1} - u_j) \right] \tag{A48}$$

REFERENCES

1. Garner, H. C.; Rogers, E. W. E.; Acum, W. E. A.; and Maskell, E. C.: Subsonic Wind Tunnel Wall Corrections. AGARDograph 109, Oct. 1966.

2. Pindzola, M.; and Lo, C. F.: Boundary Interference at Subsonic Speeds in Wind Tunnels With Ventilated Walls. AEDC-TR-69-47, U.S. Air Force, May 1969. (Available from DTIC as AD 687 440.)

3. Preston, J. H.; and Sweeting, N. E.: The Experimental Determination of the Interference on a Large Chord Symmetrical Joukowski Aerofoil Spanning a Closed Tunnel. R. & M. No. 1997, British A.R.C., 1942.

4. Preston, J. H.; Sweeting, N. E.; and Cox, D. K.: The Experimental Determination of the Two-Dimensional Interference on a Large Chord Piercy 12/40 Aerofoil in a Closed Tunnel Fitted With a Flexible Roof and Floor. R. & M. No. 2007, British A.R.C., 1944.

5. Kroeger, Richard A.; and Martin, Walter A.: The Streamline Matching Technique for V/STOL Wind Tunnel Wall Corrections. AIAA Paper No. 67-183, Jan. 1967.

6. Lo, Ching-Fang: Wind-Tunnel Wall Interference Reduction by Streamwise Porosity Distribution. AIAA J., vol. 10, no. 4, Apr. 1972, pp. 547-550.

7. Ferri, Antonio; and Baronti, Paolo: A Method for Transonic Wind-Tunnel Corrections. AIAA J., vol. 11, no. 1, Jan. 1973, pp. 63-66.

8. Sears, W. R.: Self-Correcting Wind Tunnels. Aeronaut. J., vol. 78, no. 758/759, Feb./Mar. 1974, pp. 80-89.

9. Vidal, R. J.; Erickson, J. C., Jr.; and Catlin, P. A.: Experiments With a Self-Correcting Wind Tunnel. Windtunnel Design and Testing Techniques, AGARD-CP-174, Mar. 1976, pp. 11-1 - 11-13.

10. Erickson, John C., Jr.; and Vidal, Robert J.: Wind Tunnel Wall Effects. Proj. No. NR 061-199 (Contract No. N00014-77-C-0052), Calspan Corp., [1978].

11. Chevallier, J. P.: Self-Correcting Transonic Wind Tunnel. NASA TT F-16228, 1978.

12. Chevallier, Jean-Pierre: Adaptive Wall Transonic Wind Tunnels. Windtunnel Design and Testing Techniques, AGARD-CP-174, Mar. 1976, pp. 12-1 - 12-8.

13. Goodyer, M. J.: A Low Speed Self Streamlining Wind Tunnel. Windtunnel Design and Testing Techniques, AGARD-CP-174, Mar. 1976, pp. 13-1 - 13-8.

14. Goodyer, Michael J.: The Self Streamlining Wind Tunnel. NASA TM X-72699, 1975.

15. Wolf, S. W. D.; and Goodyer, M. J.: Self Streamlining Wind Tunnel - Low Speed Testing and Transonic Test Section Design. NASA CR-145257, 1977.

16. Wolf, S. W. D.; and Goodyer, M. J.: Studies of Self Streamlining Wind Tunnel Real and Imaginary Flows. NASA CR-158831, 1979.

17. Judd, M.; Goodyer, M. J.; and Wolf, S. W. D.: Application of the Computer for On-Site Definition and Control of Wind Tunnel Shape for Minimum Boundary Interference. Numerical Methods and Windtunnel Testing, AGARD-CP-210, Oct. 1976, pp. 6-1 - 6-14.

18. Sears, W. R.: Some Experiences With the Exploitation of Measurements of the Perturbation Field in a Wind Tunnel To Improve Simulation. Numerical Methods and Windtunnel Testing, AGARD-CP-210, Oct. 1976, pp. 5-1 - 5-4.

19. Kraft, E. M.; and Dahm, W. J. A.: Direct Assessment of Wall Interference in a Two-Dimensional Subsonic Wind Tunnel. AIAA-82-0187, Jan. 1982.

20. Liepmann, H. W.; and Roshko, A.: Elements of Gasdynamics. John Wiley & Sons, Inc., c.1957.

21. Churchill, Ruel V.; Brown, James W.; and Verhey, Roger F.: Complex Variables and Applications, Third ed. McGraw-Hill Book Co., c.1974.

22. Bristow, D. R.: Development of Panel Methods for Subsonic Analysis and Design. NASA CR-3234, 1980.

23. Ladson, Charles L.: Description and Calibration of the Langley 6- by 19-Inch Transonic Tunnel. NASA TN D-7182, 1973.

24. Newman, Perry A.; and Anderson, E. Clay: Numerical Design of Streamlined Tunnel Walls for a Two-Dimensional Transonic Test. NASA TM-78641, 1978.

25. Newman, Perry A.; and Anderson, E. Clay: Analytical Design of a Contoured Wind-Tunnel Liner for Supercritical Testing. Advanced Technology Airfoil Research, Volume I, NASA CP-2045, Part 2, 1979, pp. 499-509.

26. Weast, Robert C., ed.: Handbook of Tables for Mathematics, Revised Fourth ed. CRC Press, Inc., 1975.

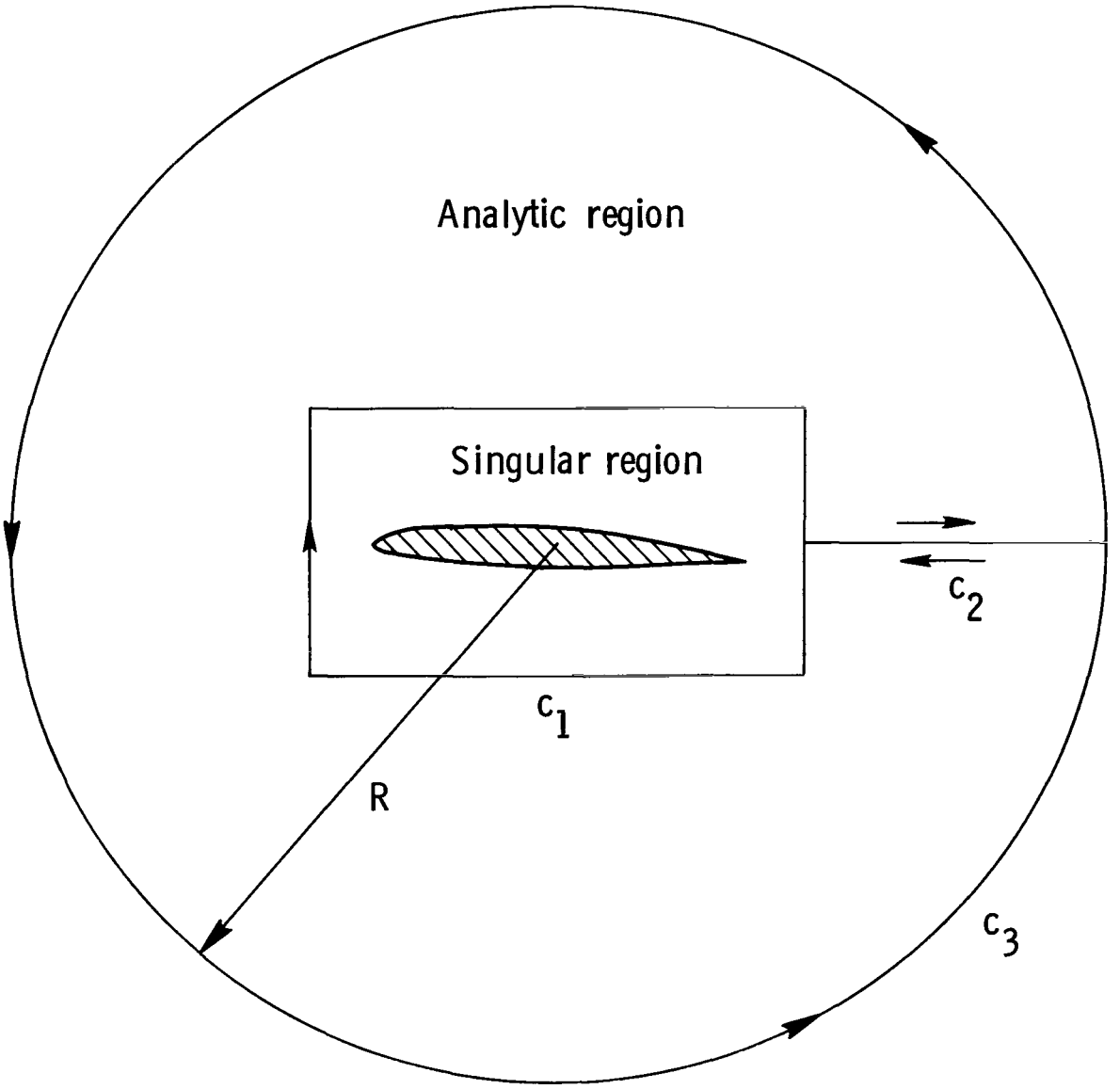

Figure 1.- Contour used for evaluation of equation (7).

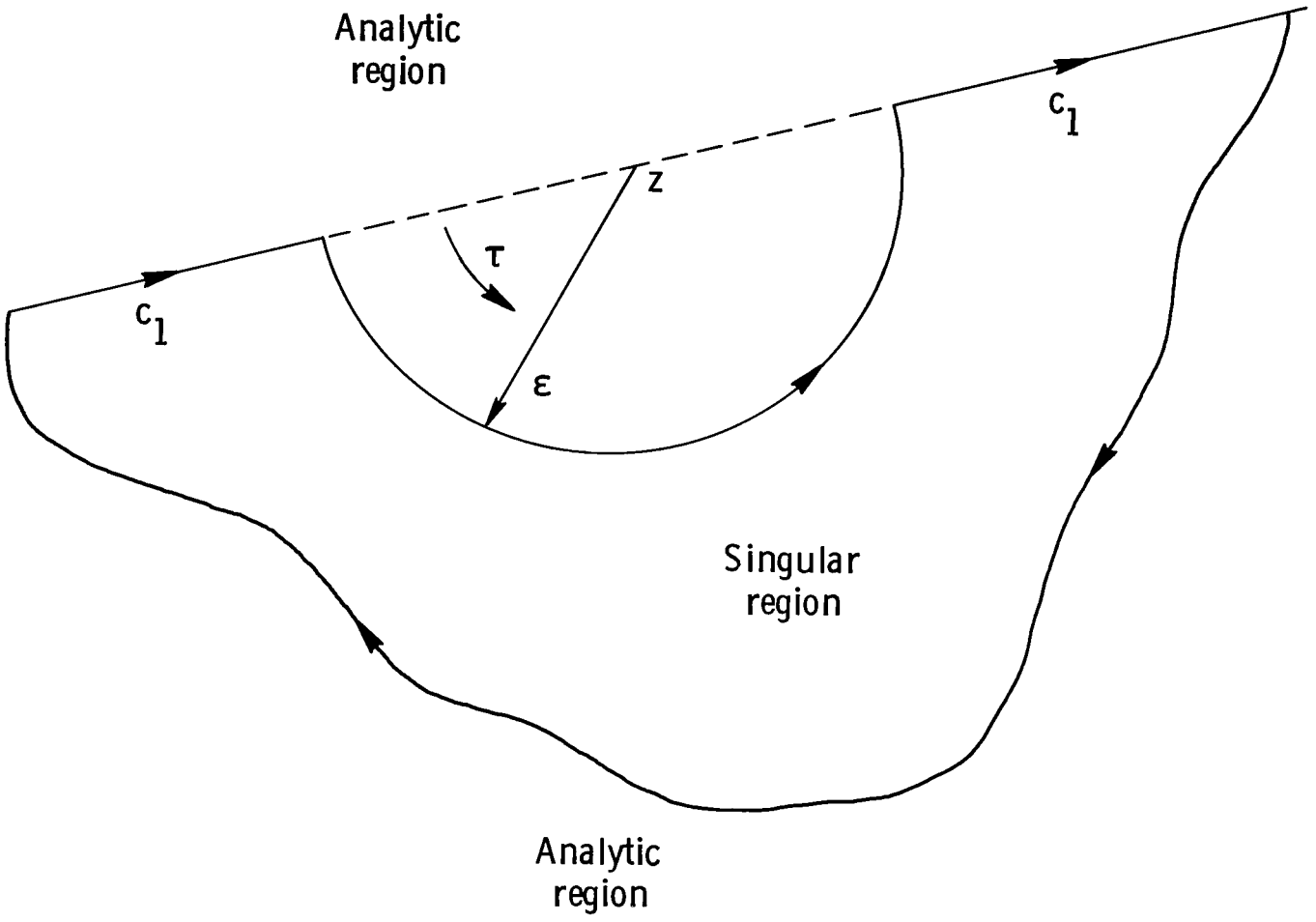

Figure 2.- Indented contour used for evaluation of equation (8) as z approaches the boundary c_1.

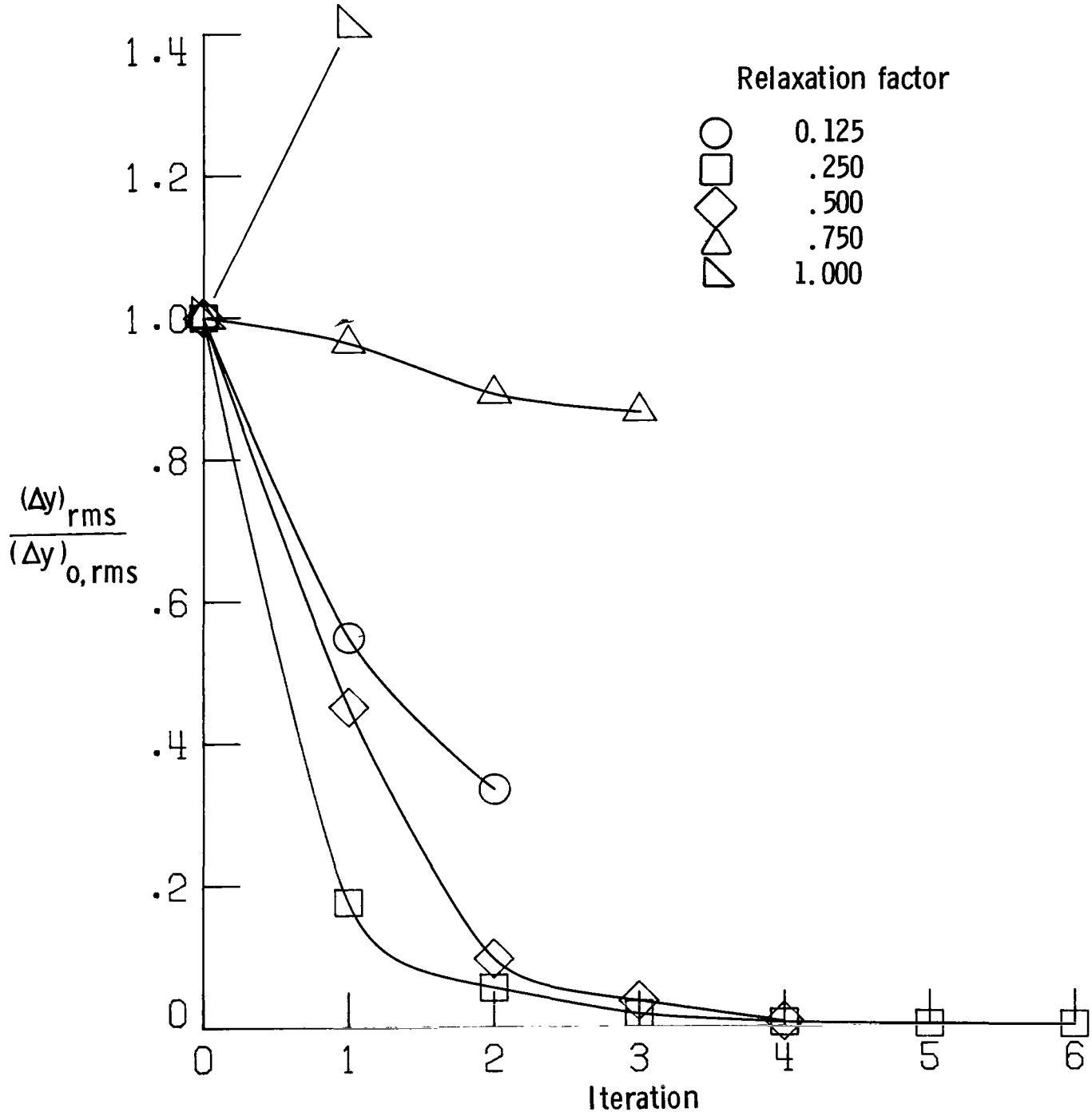

Figure 3.- Circular-cylinder convergence characteristics.

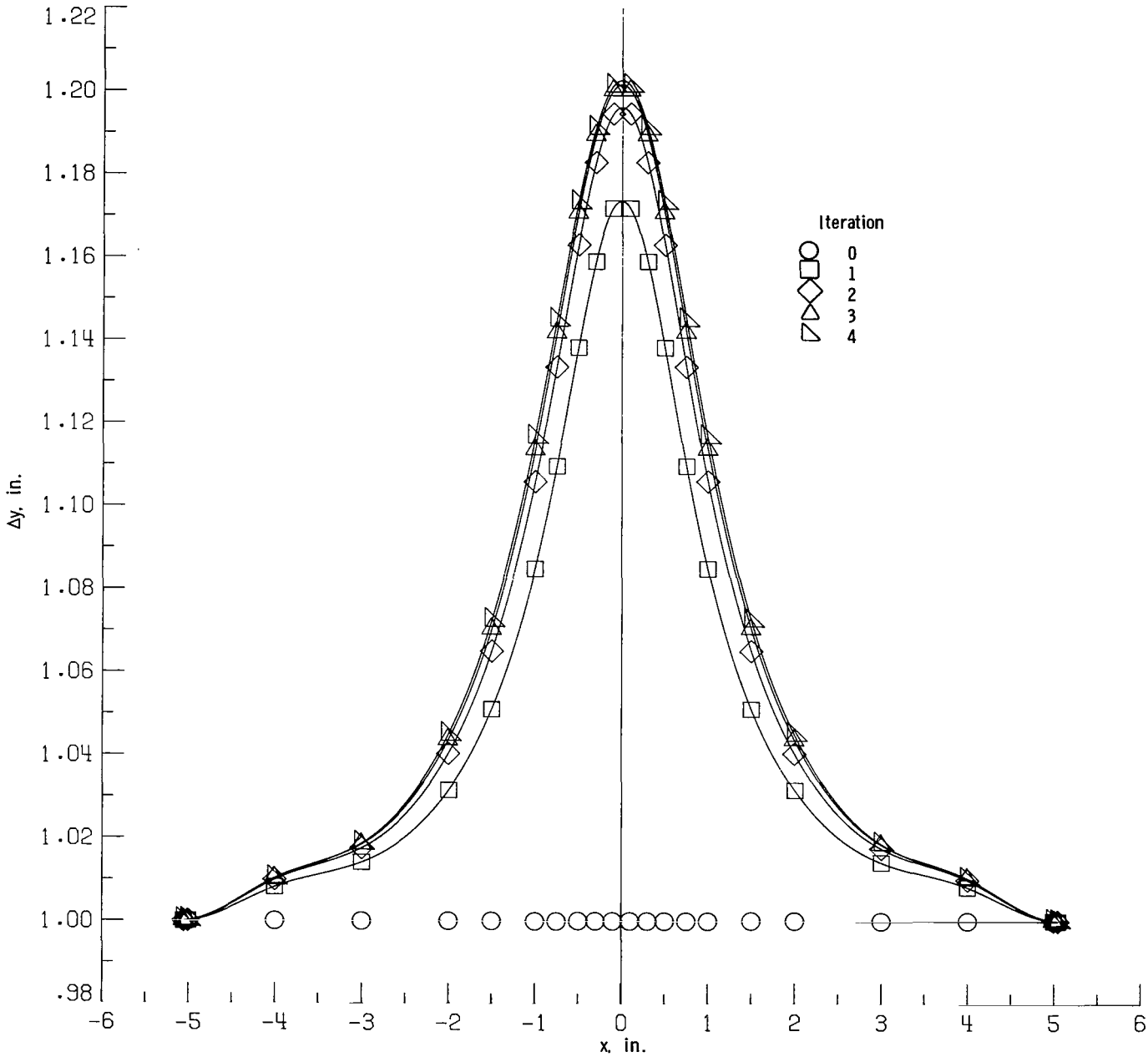

Figure 4.- Flexible-wall settings for circular cylinder. Relaxation factor, 0.25.

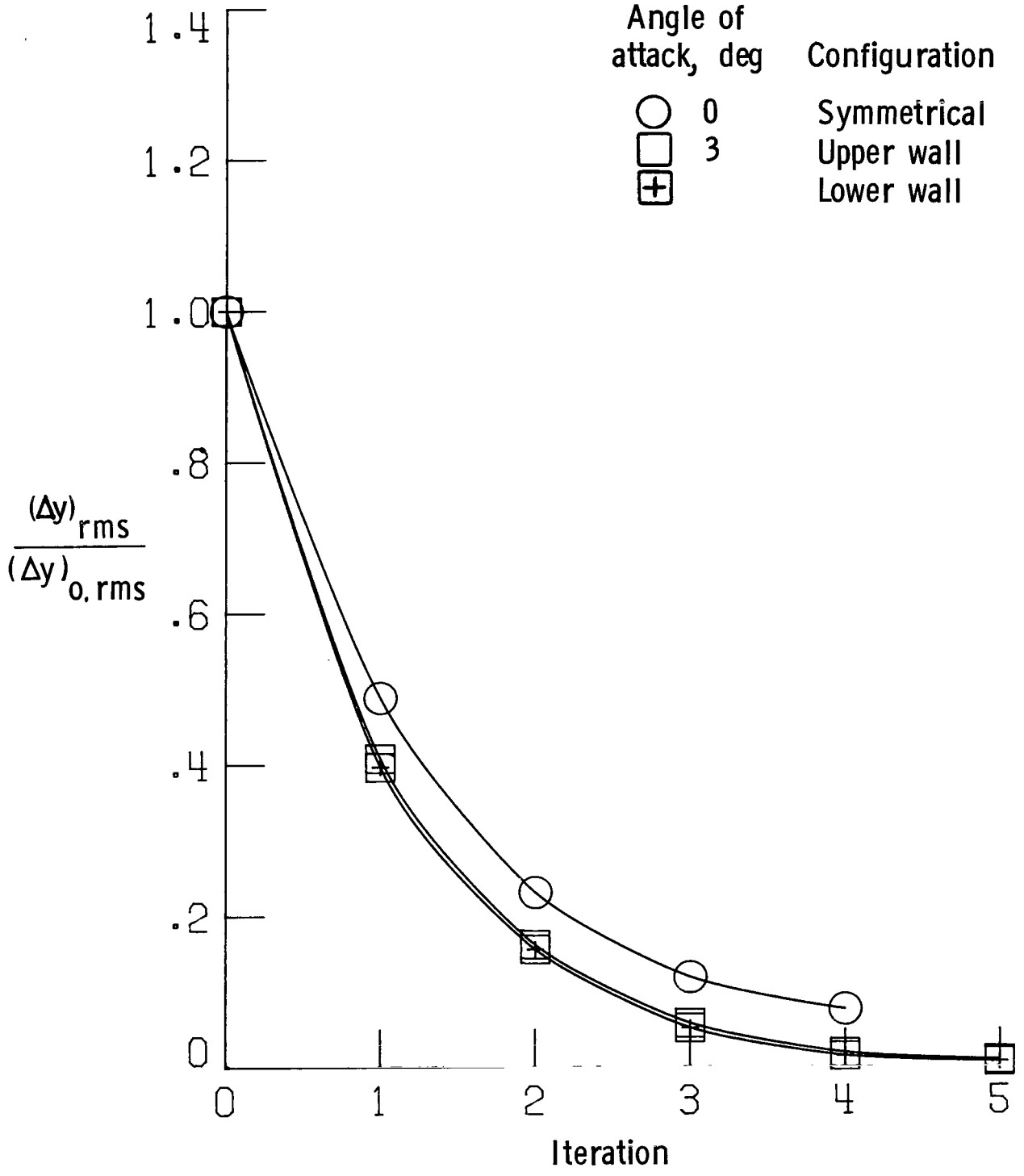

Figure 5.- Flexible-wall convergence characteristics for an NACA 0012 airfoil.

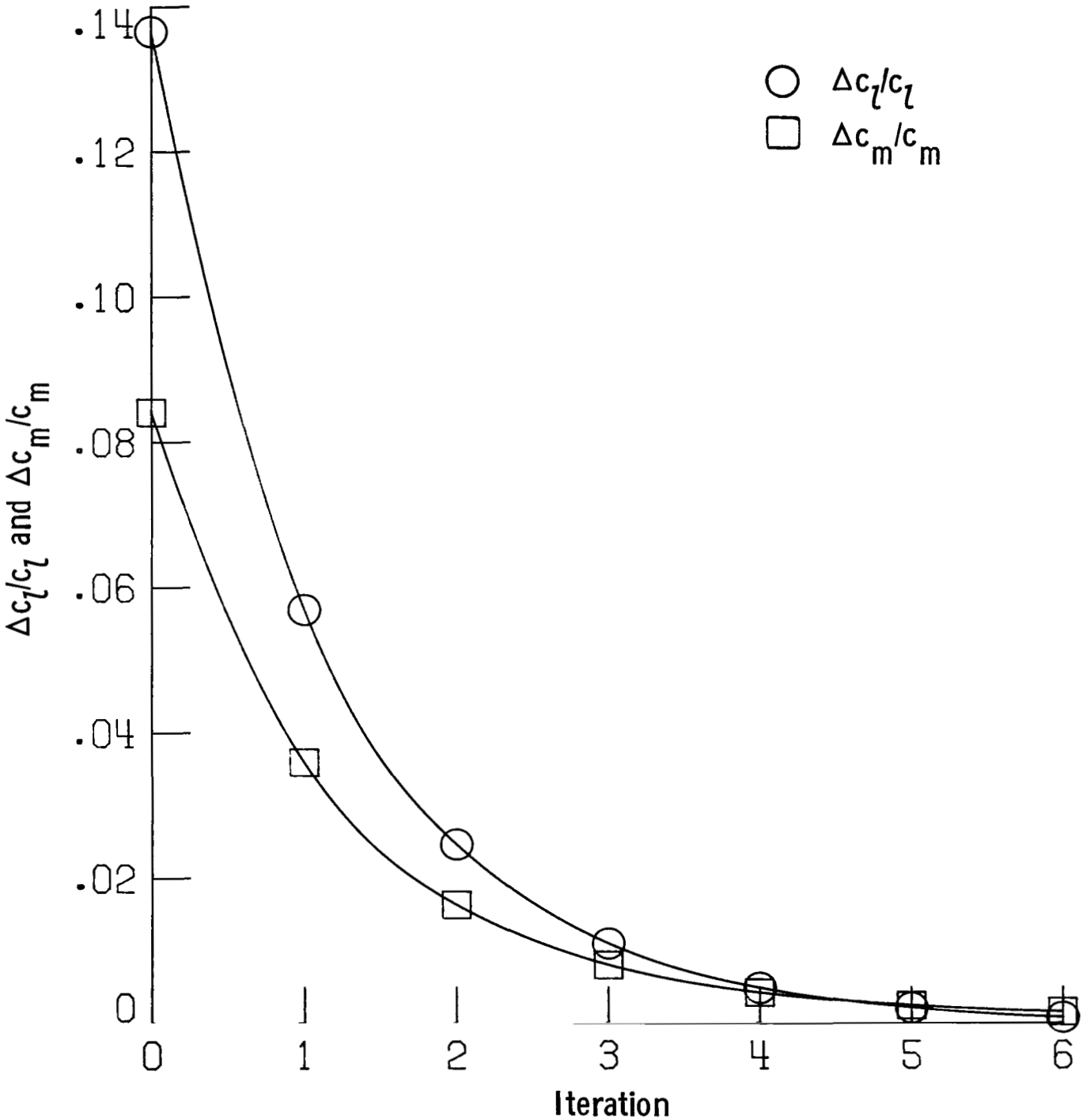

Figure 6.- Convergence of force coefficients of an NACA 0012 airfoil at an angle of attack of 3°.

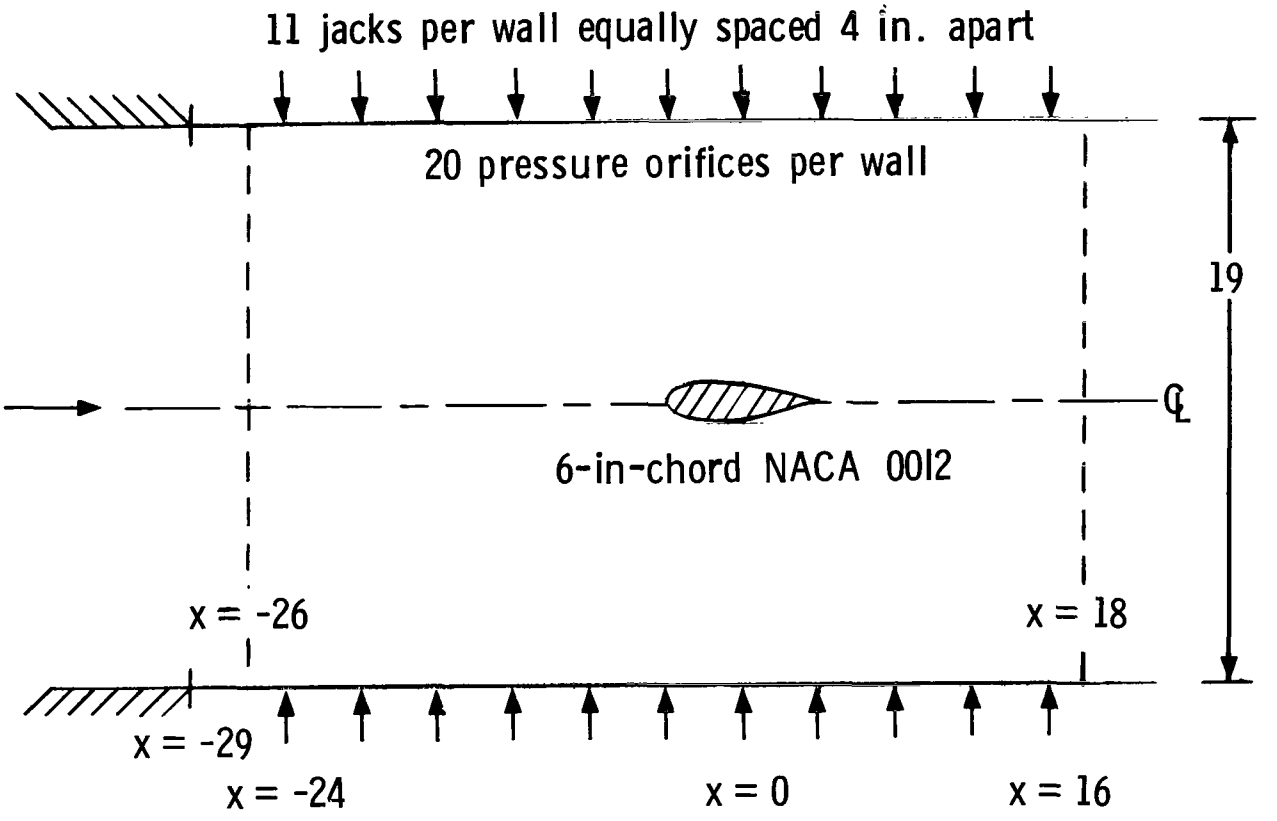

Figure 7.- Schematic drawing of flexible-wall tunnel. Dimensions are in inches.

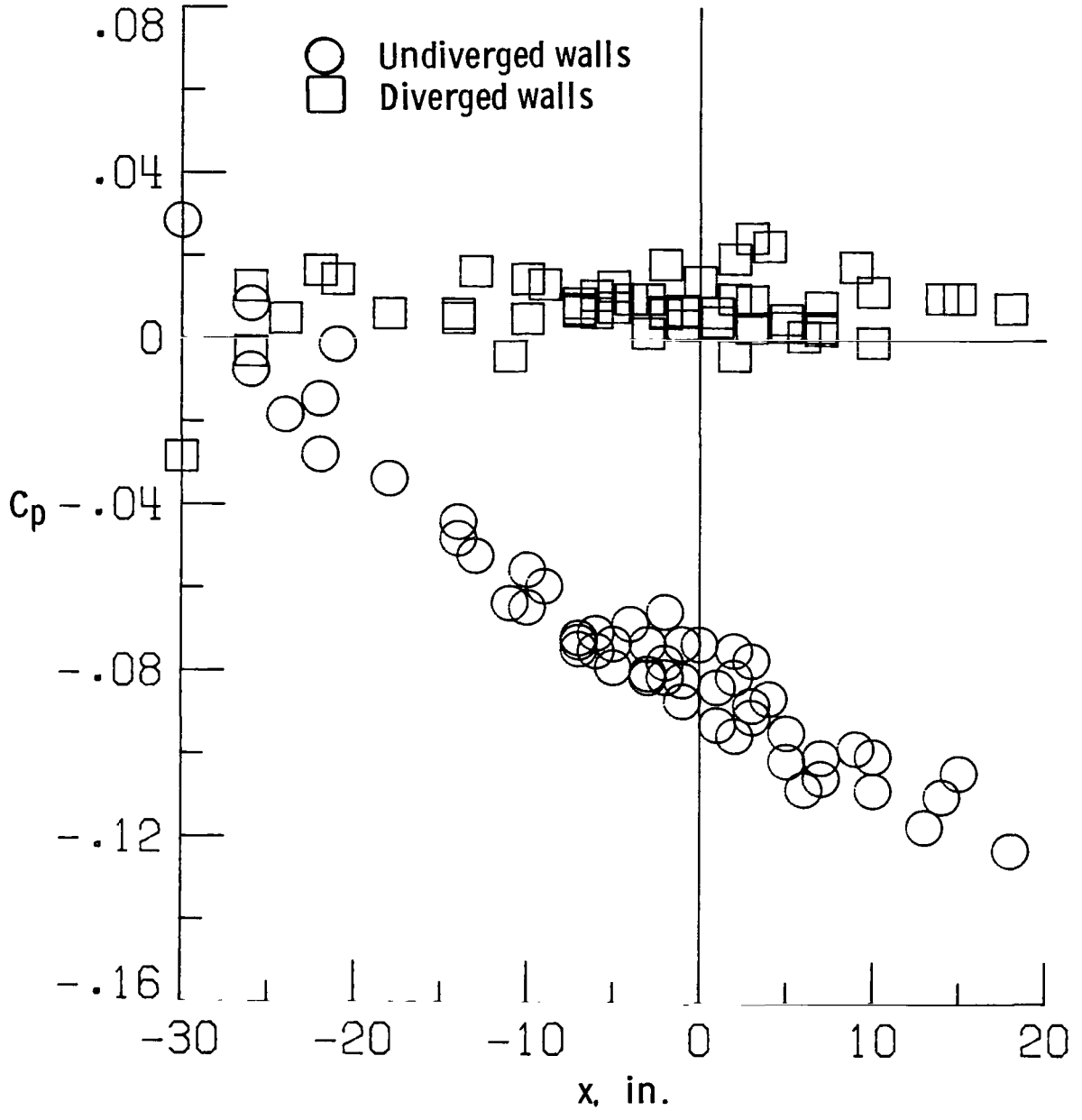

Figure 8.- Tunnel-empty flexible-wall calibration for diverged and undiverged walls. $M \approx 0.71$.

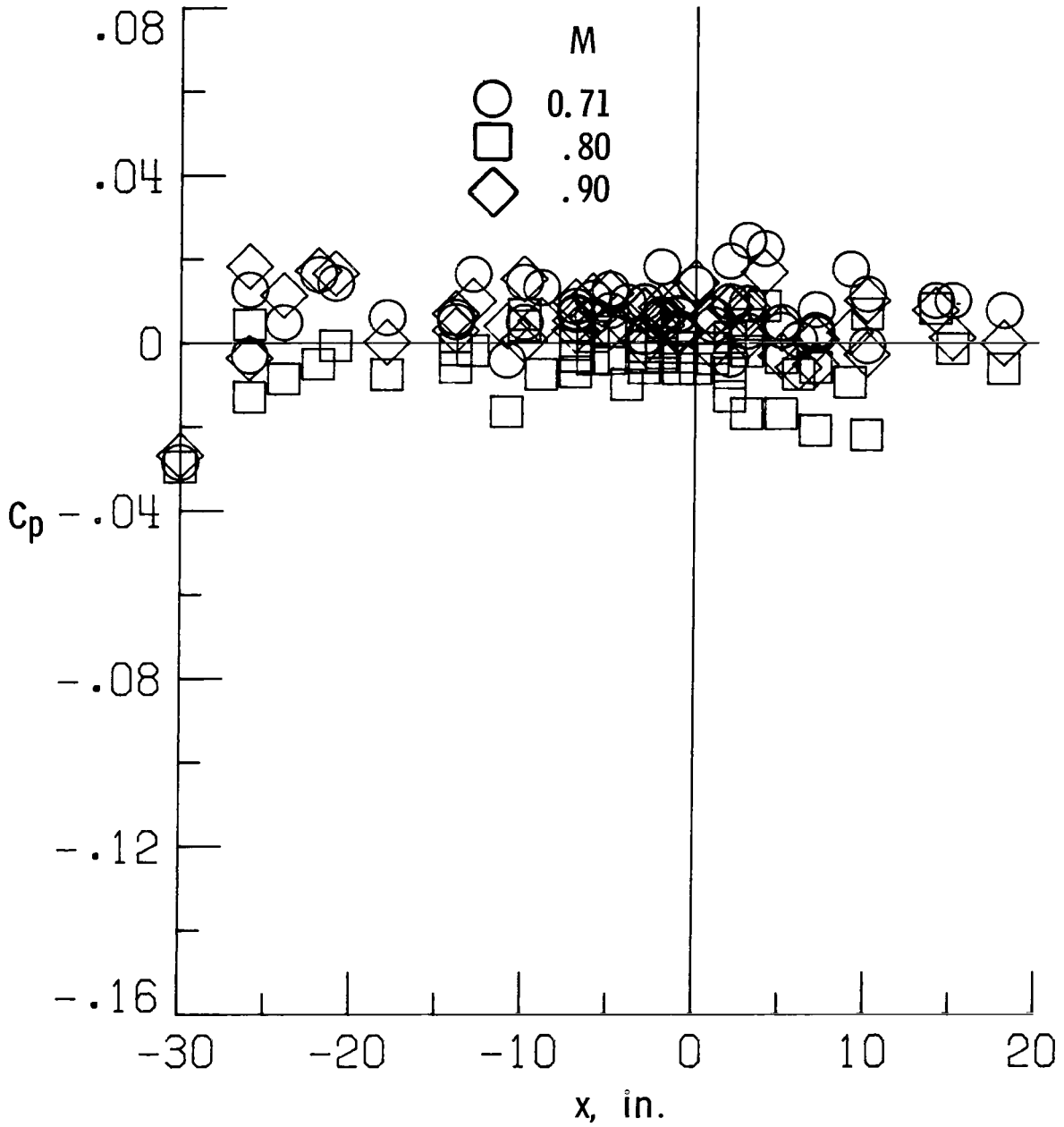

Figure 9.- Tunnel-empty flexible-wall calibration for diverged walls.

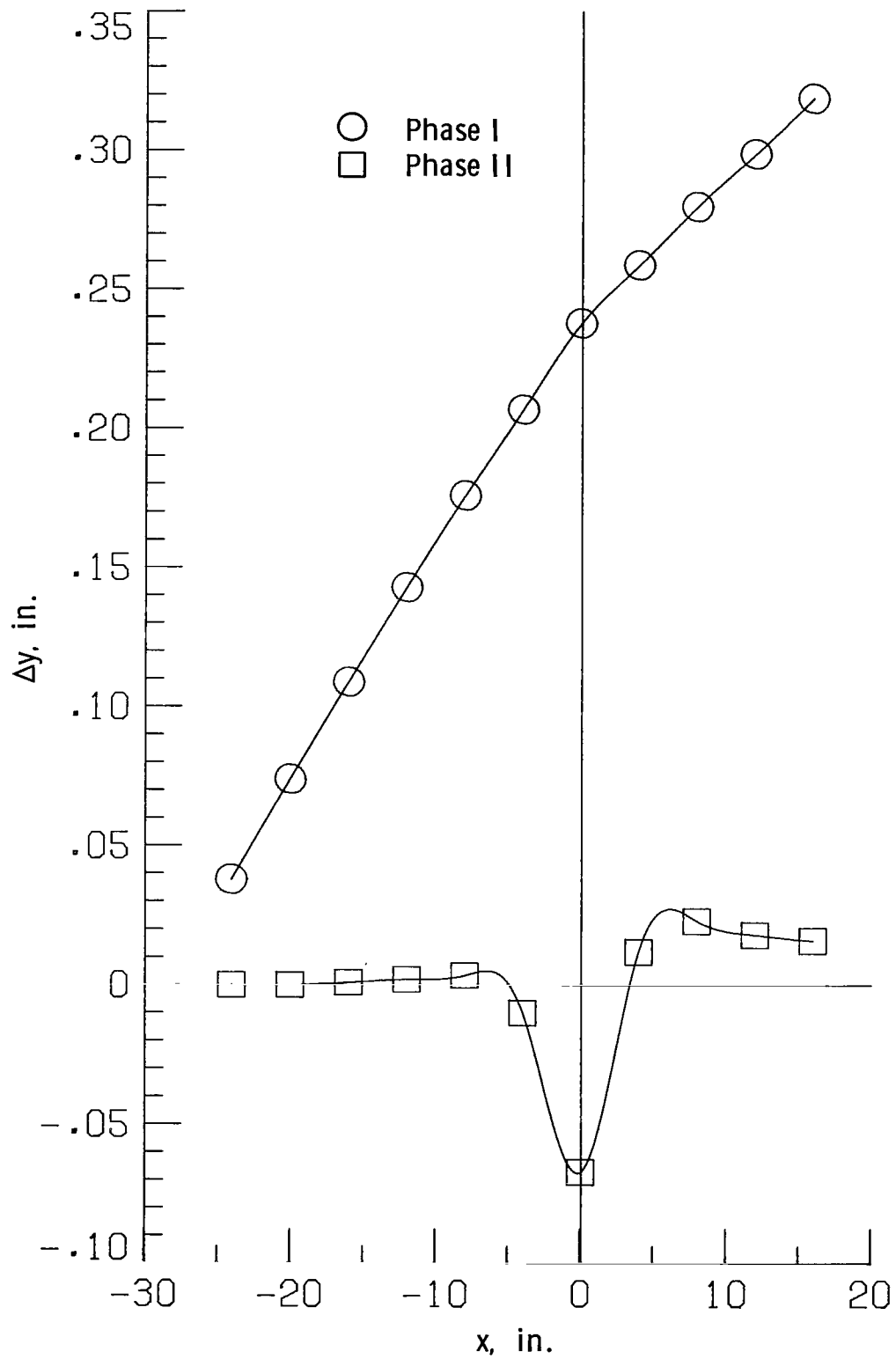

Figure 10.- Viscous corrections. $M_\infty = 0.767$.

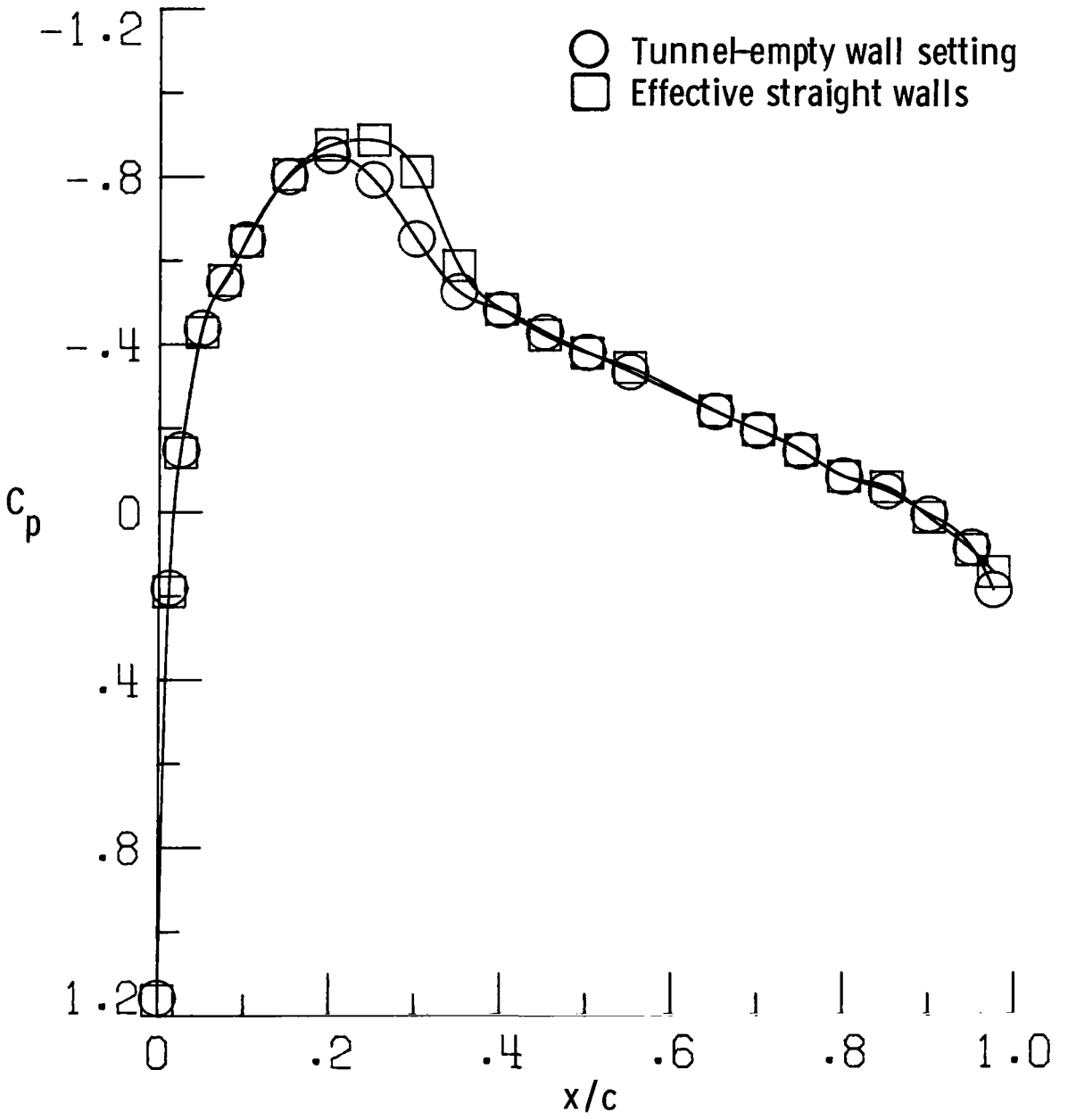

Figure 11.- Comparison of airfoil pressures with viscous corrections to flexible walls at $M_\infty = 0.77$.

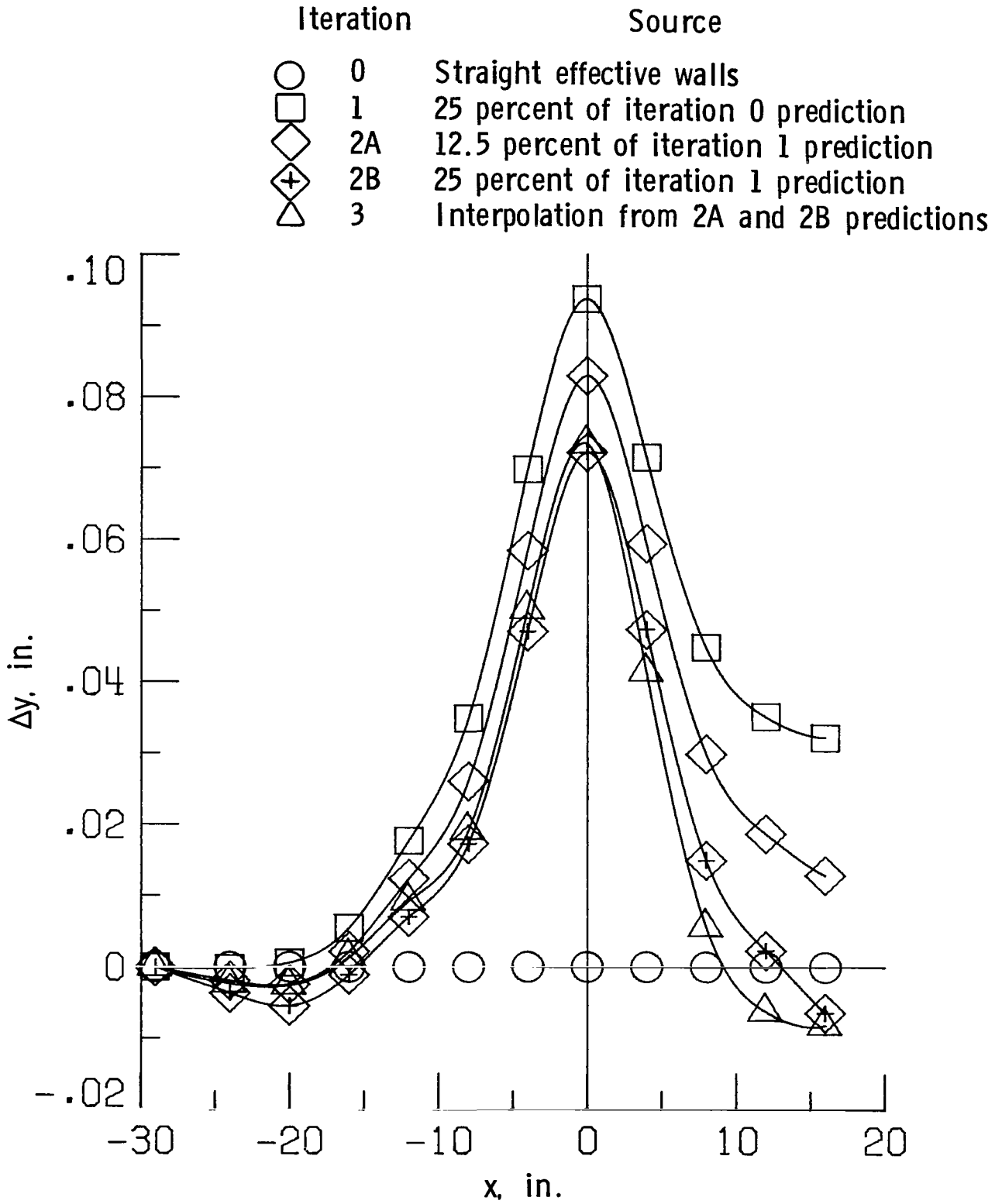

Figure 12.- Comparison of flexible-wall iterative locations at $M_\infty = 0.77$.

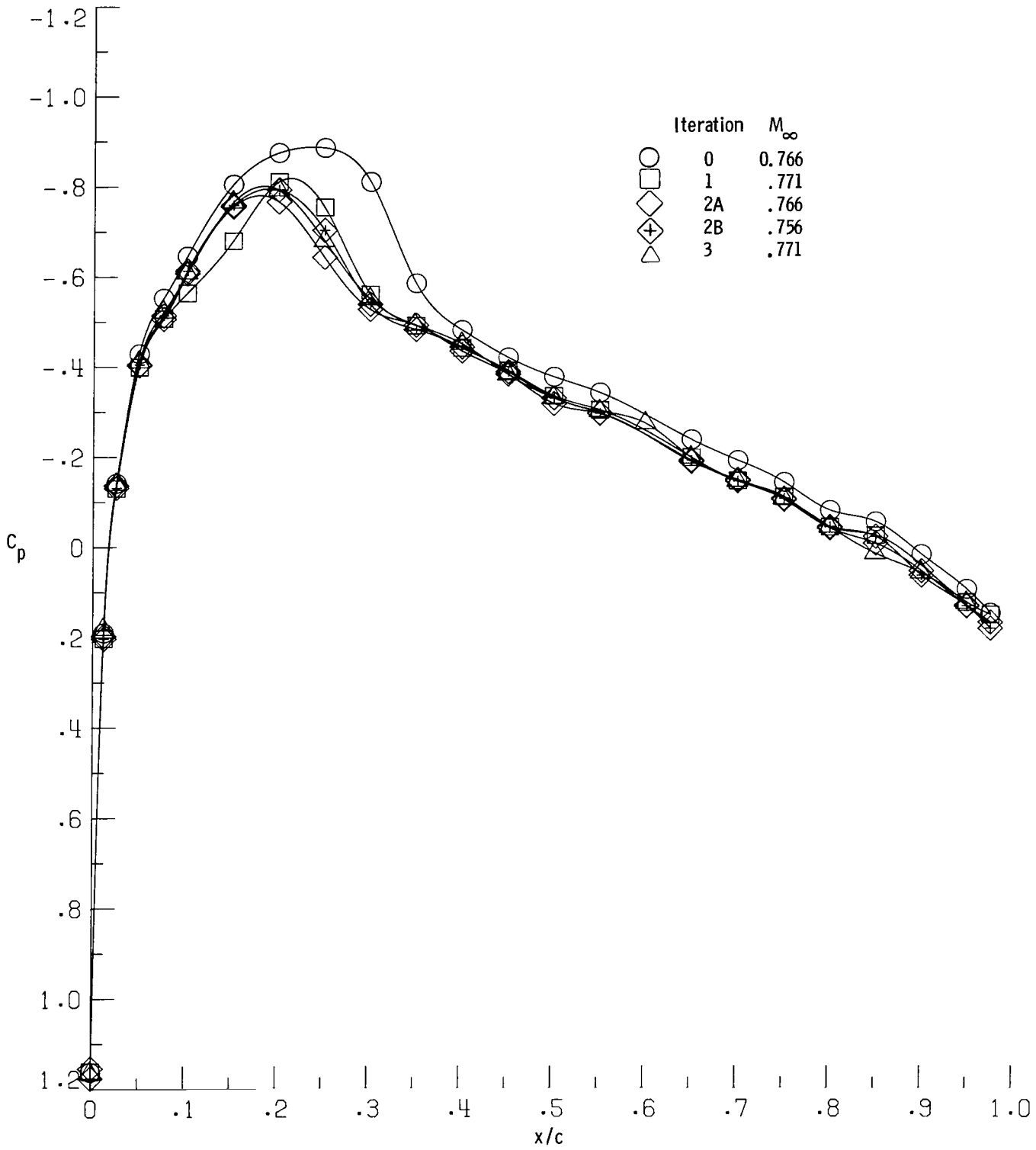

Figure 13.- Comparison of iterative airfoil pressure distributions.

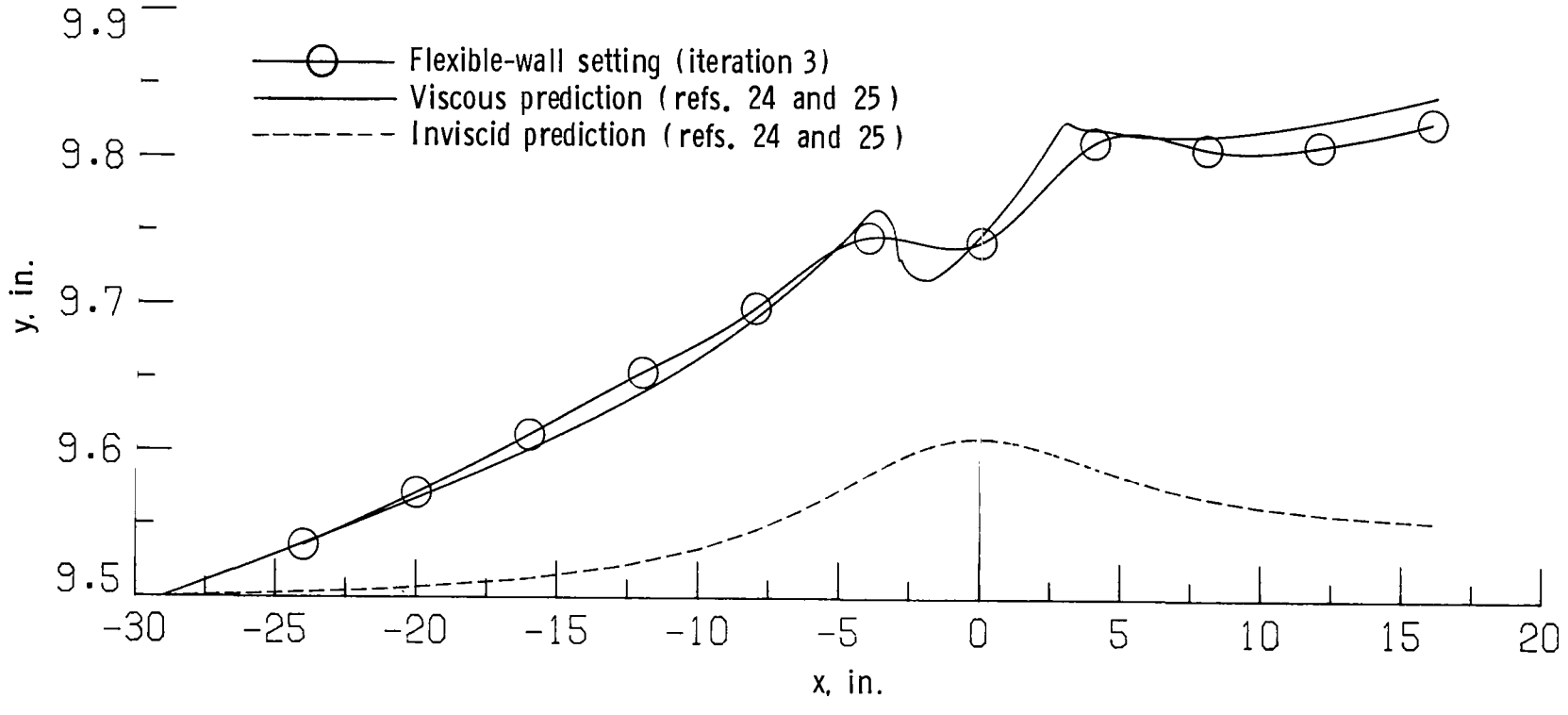

Figure 14.- Comparison of final results with Newman-Anderson theory (refs. 24 and 25) for an NACA 0012 airfoil. $M_\infty = 0.77$; $R_{chord} = 3.07 \times 10^6$.

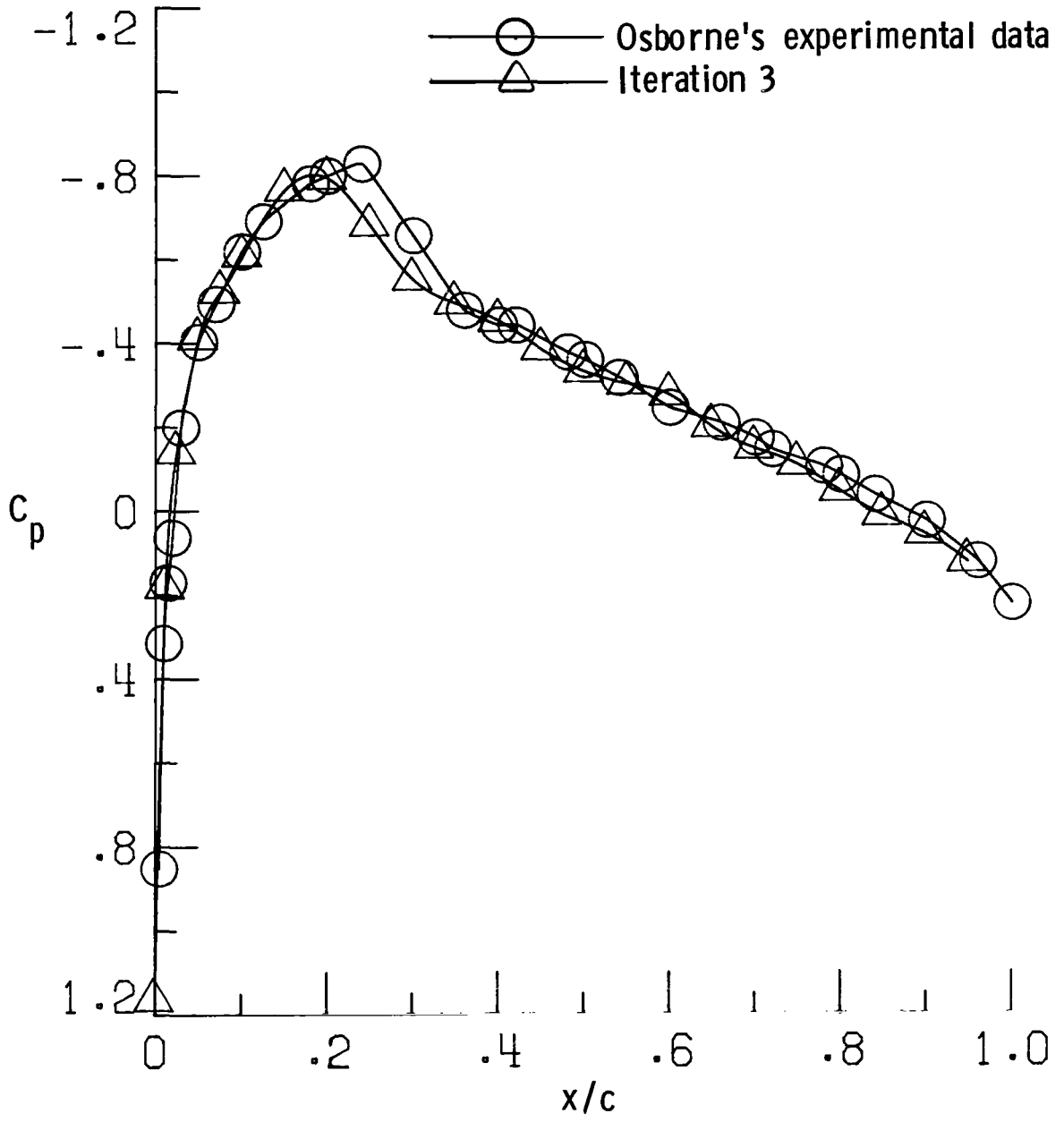

Figure 15.- Comparison of final airfoil results with Osborne's experimental data for an NACA 0012 airfoil. $M_\infty = 0.767$; $R_{chord} = 3.07 \times 10^6$.

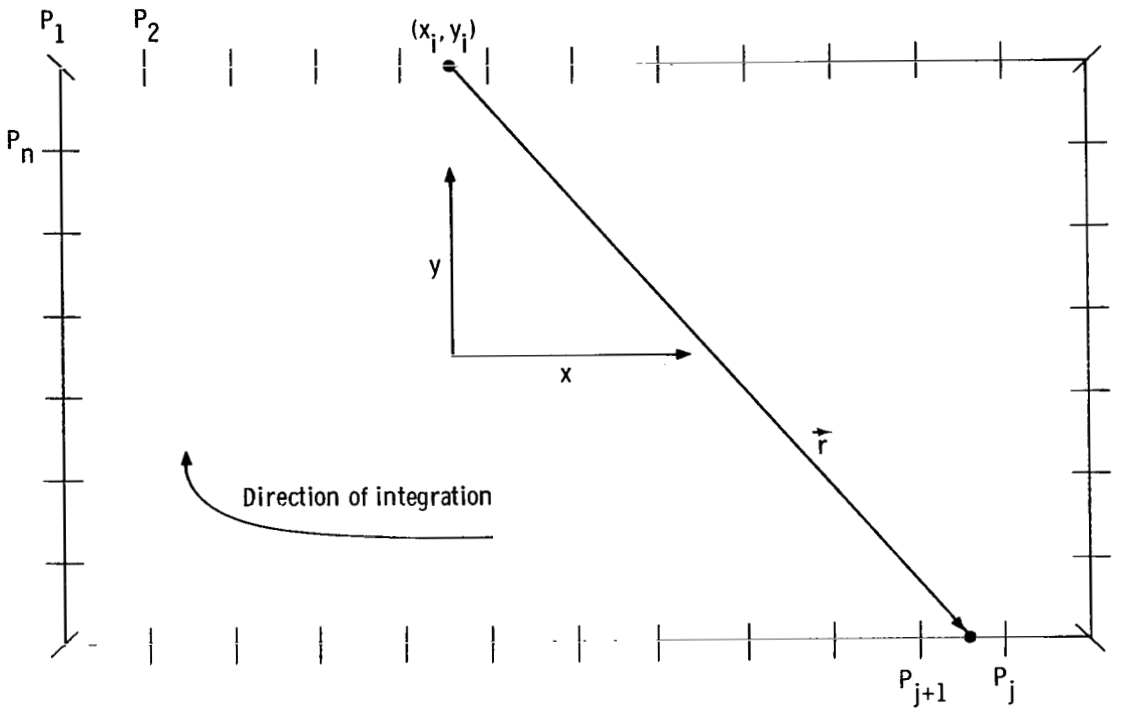

(a) Discretized wind-tunnel-wall contour.

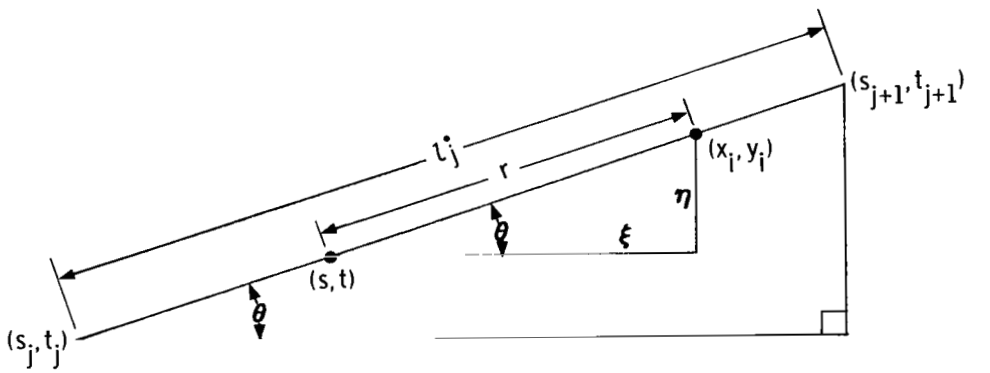

(b) Singular-wall-strip notation.

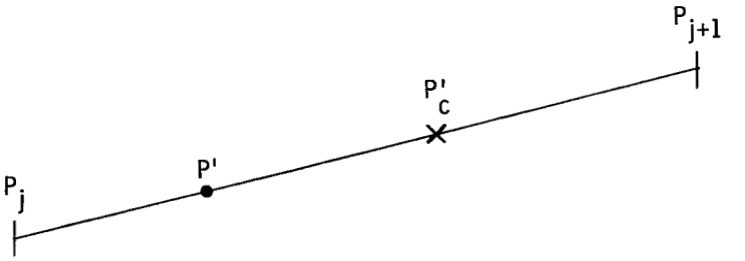

(c) Singular wall strip.

Figure 16.- Wind-tunnel wall and nomenclature.

1. Report No.	2. Government Accession No.	3. Recipient's Catalog No.
NASA TP-2081		

4. Title and Subtitle	5. Report Date
A METHOD FOR MODIFYING TWO-DIMENSIONAL ADAPTIVE WIND-TUNNEL WALLS INCLUDING ANALYTICAL AND EXPERIMENTAL VERIFICATION	February 1983
	6. Performing Organization Code: 505-31-33-09
7. Author(s): Joel L. Everhart	8. Performing Organization Report No.: L-15491
	10. Work Unit No.
9. Performing Organization Name and Address: NASA Langley Research Center, Hampton, VA 23665	11. Contract or Grant No.
	13. Type of Report and Period Covered: Technical Paper
12. Sponsoring Agency Name and Address: National Aeronautics and Space Administration, Washington, DC 20546	14. Sponsoring Agency Code

15. Supplementary Notes

This work was initiated while the author was a graduate research scholar assistant in The George Washington University Joint Institute for Advancement of Flight Sciences.

16. Abstract

The theoretical development of a simple and consistent method for removing the interference in adaptive-wall wind tunnels is reported. A Cauchy integral formulation of the velocities in an imaginary infinite extension of the real wind-tunnel flow is obtained and evaluated on a closed contour dividing the real and imaginary flow. The contour consists of the upper and lower effective wind-tunnel walls (wall plus boundary-layer displacement thickness) and upstream and downstream boundaries perpendicular to the axial tunnel flow. The resulting integral expressions for the streamwise and normal perturbation velocities on the contour are integrated by assuming a linear variation of the velocities between data-measurement stations along the contour. In an iterative process, the velocity components calculated on the upper and lower boundaries are then used to correct the shape of the wall to remove the interference. Convergence of the technique is shown numerically for the cases of a circular cylinder and a lifting and nonlifting NACA 0012 airfoil in incompressible flow. Experimental convergence at a transonic Mach number is demonstrated by using an NACA 0012 airfoil at zero lift.

17. Key Words (Suggested by Author(s))	18. Distribution Statement
Wind tunnels Wall interference Adaptive wind-tunnel walls Transonic flow Cauchy integral formula	Unclassified - Unlimited Subject Category 09

19. Security Classif. (of this report)	20. Security Classif. (of this page)	21. No. of Pages	22. Price
Unclassified	Unclassified	46	A03

For sale by the National Technical Information Service, Springfield, Virginia 22161

NASA-Langley, 1983

National Aeronautics and
Space Administration

Washington, D.C.
20546

Official Business
Penalty for Private Use, $300

THIRD-CLASS BULK RATE

Postage and Fees Paid
National Aeronautics and
Space Administration
NASA-451

3 1 1U,A, 830218 S00903DS
DEPT OF THE AIR FORCE
AF WEAPONS LABORATORY
ATTN: TECHNICAL LIBRARY (SUL)
KIRTLAND AFB NM 87117

S

NASA

POSTMASTER: If Undeliverable (Section 158 Postal Manual) Do Not Return